Research on Le effect of Acoustic Instability in Downward Propagating Flames

(下方伝播火炎での音響学的不安定性に対する Le の影響)

Yongho Chung

Research on Le effect of Acoustic Instability in Downward Propagating Flames

By

Yongho Chung

Submitted to the Department of Mechanical and Space Engineering, Hokkaido University, Japan, in Partial Fulfillment of the Requirement for the Degree of Doctor of Philosophy in Mechanical and Space Engineering

August 2018

Abstract

An interaction between a heat release and acoustic fluctuations can cause the thermoacoustic instabilities. It is important to understand the thermoacoustic instabilities because industrial applications such as rocket engines and gas turbine are often suffering from the thermo acoustic instabilities, and it leads performance degradation, in addition to shortening its lifetime.

Among the experimental studies of thermoacoustic instabilities, flame propagation experiment in a combustion tube open at one end is among the most elementary and widely employed to describe the different types of development of acoustic instability. The primary acoustic instability is evolved from a curve flame of hydrodynamic instability region to a vibrating flat flame and the secondary instability is evolved from a flat flame to the turbulent motion via a corrugated flame. The typical feature of primary acoustic instability is that the flame shape is planar. Therefore, the Lewis number effect on acoustic instability which is contributed by flame front curvature cannot be observed in general. However, the utilization of CO_2 laser irradiation facilitates the modification of flame front shape. The research on Le effect on acoustic instability was carried out through controlling flame front shape.

In Chapter 1, briefly overview of premixed flame, intrinsic flame instabilities, and acoustic instabilities in combustion tube are elucidated. Then, an objective and a scope of this study are presented.

In Chapter 2, the experimental setup and procedure are described. The combustion tube (transparent acrylic tube, 50-mm inner diameter and 711-mm length) is fixed vertically and charged with the tested gas at atmospheric pressure. The premixed gas was composed of ethylene, oxygen, carbon dioxide, and propane. Ethylene gas is mostly used as a fuel. In some cases, ethylene and propane mixture was used to keep ethylene concentration in the gas

composition to attain constant laser absorption rate. The time-dependent behaviors of the downward-propagating flame are recorded by high-speed cameras. The temporal variation of the acoustic pressure is measured at the bottom end of the tube.

In Chapter 3, the main focus is to examine effect of Lewis number on the growth of acoustic pressure. The CO_2 laser irradiation method is applied to alter the shape of the flame front, resulting in obtainment of convex and concave curvature. The generation of convex curvature by laser irradiation can facilitate the growth of acoustic pressure for Le<1 because the concentration of the deficient reactant approaching the flame could be converged with the convex flame structure. When the laser power increases, the amplitude of the convex curvature of flame also increases. It means that the flame undergoes stronger thermal diffusive instability, resulting in the growth rate of acoustic pressure rise. For Le>1, the growth of acoustic pressure amplitude is suppressed while the flame has the convex curvature by laser irradiation. It can be also elucidated by the mechanism of diffusive thermal instability. In Le>1, the thermal diffusion process is more dominant and hence the defocusing effect of the thermal diffusion is stronger than the convergence effect of deficient reactant. It causes the local flame temperature decrease and the suppression of growth of acoustic pressure. For Le<1, the flame surface area increased as the laser power rises and beginning of laser irradiation is earlier. The coupling constant, βM, is proportional to not only the growth rate of primary acoustic instability but the normalized flame surface area. Based on experimental results of Le<1, the normalized flame area was derived and linear relationship was obtained with the growth rate of acoustic pressure.

In Chapter 4, the effect of Lewis number on the transition from primary acoustic instability to secondary acoustic instability in nonequidiffusive flame is described. The Lewis number effect is significant on the enhancement or decline of heat release, and it also leads to two distinct transition behavior: (1) the flame transits from convex flame structure to secondary acoustic instability; (2) the flame transits from concave flame structure to secondary acoustic

instability. An attempt was made to establish the stability map of the transition as a function of laser irradiation conditions. The transition criteria variation is very limited for Le<1 as a function of laser exposure time and the transition behavior is always same as (1). The transition occurs very initial moment of the period of laser irradiation because the convex curvature causes local flame temperature rise. In this scenario, the transition criteria in terms of laser exposure time cannot be sufficiently changed. Both transition behaviors were observed in Le>1 in terms of laser exposure time. In short term laser exposure cases, only convex flame front was obtained owing to shortage of laser exposure time and the transition behavior is also of (1). Therefore, the flame requires higher laser power to enable the transition due to the negative effect of Le. Once sufficient laser exposure time is given to form the concave structure, the transition begins from the concave curvature under the influence of concave flame structure.

Increasing laser power decreases the critical transition laminar burning velocities in both Le>1 and Le<1. The concave transition region in the binary fuel cases is wider than the single fuel cases. The Lewis number of binary fuel cases for fuel lean condition is larger than that of single fuel cases (1.09>1.05). It may induce easier transition for binary fuel cases. The transition criteria have very different sensitivity to the input laser power in terms of the transition modes and, even with same input laser power, the amplitude of flame front curvature is quite different between the convex and concave flames. The quantitative evaluation of curvature effect on flame burning velocity was conducted to more clarify the Lewis number effect on the transition phenomena. The result in case of concave structure is much higher than that of convex structure. It means that the effect of concave curvature is stronger than the convex curvature even under same input laser power and such relatively stronger curvature effect can cause more sensitive response of the transition criteria variation

In Chapter 5, conclusions are briefly summarized based on experimental observation.

Keywords: Acoustic instability, Growth rate, Laser irradiation, Lewis number, Primary acoustic instability, Rayleigh criterion, Secondary acoustic instability. Diffusive-thermal instability, Flame curvature

Thesis Supervisor: Osamu Fujita

Title: Professor

Acknowledgements

First of all, I would like to express my sincere gratefulness to my supervisor, Professor Osamu Fujita, for giving me a chance to study under his supervision and work at one of best laboratory. He provided me indispensable instructions, great encouragement and good guidance as well as offering the excellent research environment during my PhD course.

I wish to appreciate Professor Nozomu Hashimoto for their generous help and encouragement, and his kind comment on my research and valuable advice as the elder in life. I also thank Ms. Miho Taga for her kind help dealing a lot of paper works related to my research and business trips.

I especially want to acknowledge my master-course supervisor, Professor Jeong Park (Pukyung National University, Korea), for his continuous encouragement and extremely valuable instruction. He led me into the combustion society and scientific research. I very much appreciate him for the efforts to introduce me to the PhD course at Hokkaido University under Prof. Fujita's supervision.

I would like to thank Prof. Harunori Nagata, Prof. Nobuyuki Oshima, Prof. Nozomu Hashimoto and Prof. Osamu Fujita on evaluation committee and also for their help on my study and research. I appreciate Prof. Takashi Nakamura, Prof. Koichi Sasaki, Prof. Masao Watanabe, Prof. Terashiwa Hiroshi, Prof. Kajiwara Itsurou, Prof. Chikahisa Takemi, Prof. Ogawa Hideyuki and Prof. Totani Tsuyoshi on judgment committee.

I am very much grateful to my research group member (OFG), SungHwan Yoon, TaeJoon Noh, Ajit Kumar Dubey, Nguyen Truong Gia Tri, and Yoichiro Koyama for lots of help and academic discussion. I hope that we shall have an opportunity to study combustion research together in the future. Especially, I appreciate very much SungHwan Yoon for valuable academic advice and having personal discussion.

I would like to express my gratitude to the Ministry of Education of Japanese Government (MEXT) for providing me with financial support for 3 years as a Monbukagakusho scholarship. I also would like to express my especial thank again to my supervisor Professor Osamu Fujita for arranging the scholarship.

I warmly thank my friend, Yan Hui for their sincere friendship and help on various ways regarding life in Japan. I never forget good memory spent together and shared experiences.

I must express my very profound gratitude to my family for encouragement and supporting me throughout writing this thesis and my life in general. Lastly, I just would like to write that the degree does not belong to me, it is all of us.

Thanks to my father, mother and brother

어머니, 아버지, 그리고 동생 유빈이에게 모든 영광을 드립니다. 감사합니다.

Table of Contents

List of figures

List of tables

Nomenclature

$S_{d,lim.}$	displacement velocity enhancement by the buoyancy
g	acceleration of gravity
d	tube diameter
D	mass diffusivity of deficient species
k	wave number
L	tube length
L_b	Markstein length
S_L	laminar burning velocity
S_0	unstretched burning velocity in upstream
T_0	temperature in unburned mixture
T_b	adiabatic flame temperature
U_0	flow velocity in unburned mixture
U_b	flow velocity in burned mixture
U_n	flow velocity of normal direction in unburned mixture
U_{ll}	flow velocity of tangential direction in unburned mixture
q'	heat flux fluctuation
p'	pressure fluctuation
U_a	acoustic velocity
R_f	radius of a segment of the deformed flame
u_0	laminar burning velocity
S^l	unstretched laminar burning velocity
S_n	local flame velocity

Greek Symbols

α	thermal diffusivity
δ_f	flame thickness
κ	flame stretch rate
λ	wavelength of sound
ρ	density
ρ_b	density in burned mixture
ρ_0	density in unburned mixture
σ_{DL}	growth rate of D–L instability
Φ	equivalence ratio
θ	angle

Dimensionless Numbers

β	dimensionless activation energy or Zel'dovich number
Le	Lewis number ($=\alpha/D$)
Ma	Markstein number ($=L_b/\delta_f$)
γ	reduced gas expansion factor

Chapter 1: Introduction

1.1 Overview of premixed flame

In a combustible fuel-oxidizer mixture, once ignition is achieved, the premixed flame tends to propagate the unburned mixture and consume it as a wave phenomenon. Reacting phenomenon of well-mixed fuel and oxidizer mixture can be generally classified to two possible categories: (1) Deflagration: a combustion wave propagating at subsonic speed, (2) Detonation: a combustion wave propagating at supersonic speed. For deflagration, the chemical reaction gives a heat source to the unburned mixture by thermal diffusion. The present thesis is focused on deflagration wave only.

The steady propagation with planar, a simple framework of premixed flame structure, one-step high-activation energy kinetics, adiabatic condition is considered. The typical 1-D premixed flame structure is illustrated in Fig. 1.1. The flame structure consists of two distinct zones, namely the preheat zone which is a nonreacting convective-diffusive zone, and the reaction zone that is highly peaked and consisting of a rapidly increasing portion due to activation of the reaction. Most of chemical reaction take place in the reaction zone then implies that the heat source is supplied to the preheat zone by diffusion process in adiabatic condition, particularly.

In practical, the flame surface undergoes the aerodynamic straining owing to both incoming flow of unburned mixture and leaving flow of burned gas. For instance, the Bunsen flame has a highly curved concave structure toward the unburned mixture; a spherical flame has the convex curvature. Even if the flame is planar, the flame front is strongly affected by the aerodynamic effect. The aerodynamic effect as a function of the flow rate and flame shape, namely the flame stretch rate, is expressed as below [1]:

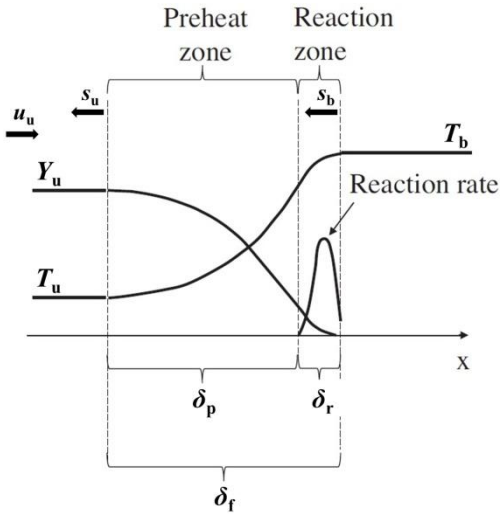

Fig. 1.1 Schematic of the premixed flame structure.

$$\kappa = \nabla_t \cdot v_{s,t} + (V_f \cdot n)(\nabla \cdot n) \tag{1-1}$$

for various geometries, where V_f is the velocity of flame surface and $v_{s,t}$ indicates the tangential component of flow velocity. $(\nabla \cdot n)$ in the second term of (Eq. 1-1) presents the flame curvature. The n is the normal vector of the flame surface. For the stationary that means no propagation and/or the planar flame, the second term can be negligible. The burning velocity of the stretched flame, Sn, has a linear relationship with stretched rate (or flame curvature). The relation is expressed by

$$S^1 = L_b \kappa + S_n \tag{1-2}$$

, where S^1 indicates unstretched burning velocity. It was characterized by the Markstien length (L) that measures the mixture`s sensitivity to the stretch rate. The linear increase in the burning velocity is identified as a function of the stretch rate as shown in Eq. 1-2.

1.2 Flame instabilities in premixed combustion

This section introduces general knowledge of intrinsic flame instabilities in premixed combustion system. The premixed flame essentially goes through unstable processes without any forced instabilities such as external flow field, acoustic sound by external input, and pressure wave by forced vibration. Such intrinsic instabilities can be categorized as hydrodynamic (Darrieus-Landau), body force (Rayleigh-Taylor), and diffusive-thermal instabilities. In premixed combustion system, above three types of flame instabilities closely interact with each other. Therefore, the mechanisms of each instability are discussed in detail.

1.2.1 Body force instability

The buoyancy-driven instability, known as the Rayleigh-Taylor instability, is caused by gravitational force. It occurs for fluids that have negative density layers in the direction of gravity. An upwardly propagating flame is an appropriate condition for development of the R-T instability. The displacement velocity of upward propagating flame is accelerated by buoyancy effect. The acceleration of the flame velocity is determined as [2]:

$$S_{\mathrm{d,lim.}} = 0.33\sqrt{gd}. \tag{1-3}$$

Here, g represents acceleration of gravity and d is characteristic length.

In case for downward propagating flames, however, the effect of body force instability is not so serious because the buoyancy flow is structurally stable and the displacement velocity is also very similar to the laminar burning velocity.

1.2.2 Hydrodynamic instability

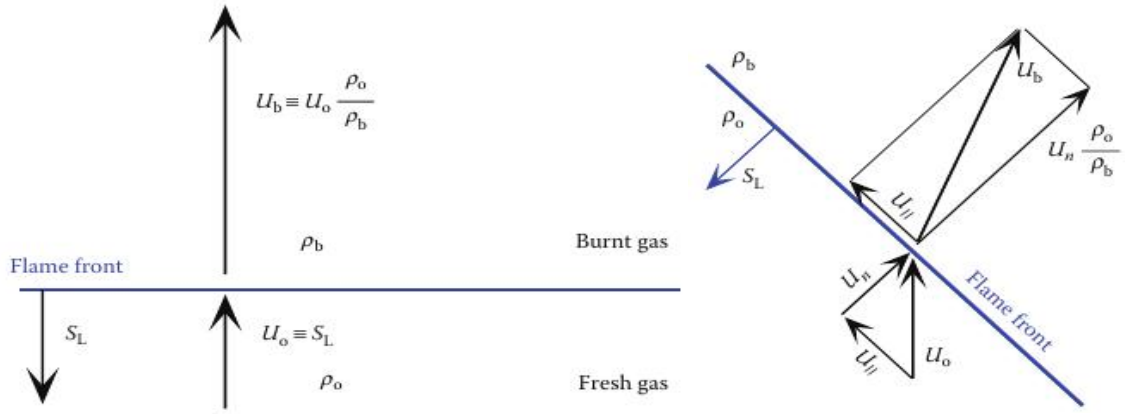

(a) (b)

Fig. 1.2 Gas expansion through (a) a planar flame and (b) an inclined flame in Ref. [5].

The premixed flames are unstable to a hydrodynamic instability that is mainly caused by the gas expansion through the exothermal reaction. It was firstly recognized by George Darrieus and Lev Landau [3-4], and it is generally referred to as the Darrieus-Landau instability.

Consider a planar premixed flame front as shown in Fig. 1.2(a), and the flame thickness is assumed to be infinitely thin (very large activation energy). The unburned mixture at temperature and density, (T_0, ρ_0), is transformed into hot burnt mixture at temperature, T_b, and density, ρ_b. The unburned mixture enters the front at speed $U_0 = S_0$, and the burnt mixture leave the front at velocity $U_b = S_L(\rho_0/\rho_b)$ because of thermal expansion. The density ratio, ρ_0/ρ_b, is roughly equal to the temperature ratio, and is of the order of 6~7 for standard hydrocarbon-air flames. This velocity jump must bring about a small pressure jump at the discontinuity interface considering momentum conservation as below:

$$\delta p = \frac{1}{2}(\rho_b u_b^2 - \rho_u u_u^2) \equiv \frac{1}{2}(\rho_u S_L^2)(\frac{\rho_u}{\rho_b} - 1). \quad (1\text{-}4)$$

The pressure jump, δp, is typically of the order of 1 Pa.

In case of the inclined flame front as shown in Fig. 1.2(b), the incoming flow consists of two vector components that are a normal velocity to the front, U_n, and a tangential velocity to

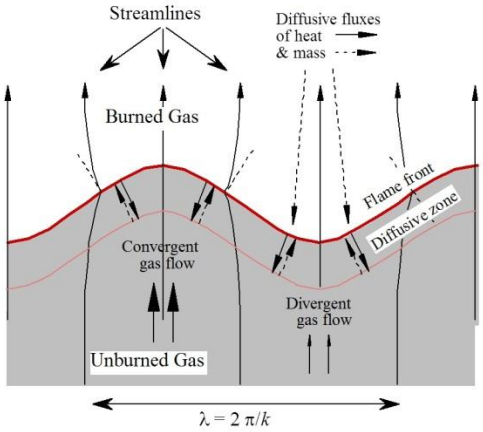

Fig. 1.3 Structure of a wrinkled flame front showing the hydrodynamic streamlines and the diffusive fluxes of heat and mass in Ref. [6].

the front, U_{ll}. The burnt mixture leaving the flame can be also decomposed into the normal and tangential components. The normal component must be equal to $U_b = S_L(\rho_0/\rho_b)$ owing to gas expansion. However, the tangential one is not changed. Therefore, the incoming flow deviates towards the outgoing normal.

Figure 1.3 shows the hydrodynamic streamlines and the diffusive fluxes of heat and mass in a wrinkled flame front. The flow of unburned gas in the vicinity of the flame front diverges and converges at convex and concave towards the fresh mixture respectively. The growth rate of the D–L instability is presented through the function of wave number, laminar burning velocity, and gas expansion ratio as [4]:

$$\sigma_{\mathrm{DL}} = kS_L\left(\frac{E_{\mathrm{ex.}}}{E_{\mathrm{ex.}}+1}\sqrt{\frac{{E_{\mathrm{ex.}}}^2+E_{\mathrm{ex.}}-1}{E_{\mathrm{ex.}}}}-1\right). \tag{1-5}$$

, where $k \equiv 2\pi/\lambda$ is the wave number. λ is the wave length of wrinkled flame front, and E is the gas expansion ratio, $\mathrm{E} = \rho_0/\rho_b$. This analysis in only valid in case that the flame front is wrinkled with moderate amplitude and the wave length is significantly larger than flame thickness.

1.2.3 Diffusive-thermal instability

In premixed flame propagation with a high activation energy, the flame propagation can be controlled by the diffusion of the heat of combustion and species. If the flame is curved or wrinkled, the gradient of temperature and mass concentration are no longer parallel to the normal direction of propagation and then the local flame velocity can change.

For concave tip toward the unburnt gas as shown in Fig. 1.3, the heat flux is locally convergent. Then the local flame temperature increases and the local propagation velocity also increases (indicated as the solid arrow in Fig. 1.3). On the other hand, the reactant is defocused simultaneously, leading in turn to a decrease in the local propagation velocity. By same reasoning as the above, for convex structure, the heat is defocused and the reactant in the vicinity of the flame front is focused. The result of two diffusive processes depend on the ratio of the thermal, α, and mass diffusion coefficient of deficient reactant, D. It is called the Lewis number,

$$Le = \alpha/D. \tag{1-6}$$

If the Lewis number is larger than unity, the heat diffusion is preponderant parameter in the propagation mechanism and the flame will be thermo-diffusively stable. Conversely the flame is cellularly unstable for $Le<1$. It can be interpreted on basis of the different diffusivities of the deficient and abundant species, leading to the conclusion that a flame is diffusively unstable if it is deficient in the more mobile reactant. This instability is referred to nonequidiffusional instability.

1.3 Acoustic instability in combustion tube

Thermo acoustic instabilities due to an interaction between heat released by the flame and acoustic fluctuations have been being an encumbrance to development of industrial applications such as gas turbines and rocket engines. It is therefore important to suppress the instabilities. The first suggestion of criterion of acoustic instability was developed by Rayleigh [7]. The suggestion was that the acoustic wave is amplified by the thermal energy if changes in heat release are in phase with the acoustic wave. The criterion can be expressed as follows:

$$\int p'q'dv > 0. \tag{1-7}$$

Where, p' and q' indicate pressure and heat release rate per unit volume respectively. This criterion is often used to elucidate the experiment data and the driving mechanisms. There have been two potential coupling mechanisms of acoustic instability, the direct sensitivity of the chemical reaction rate to the pressure wave [8-13] and the periodic fluctuation of the total flame area induced by acoustic acceleration [14-17].

In this section, the different types of acoustic instability which observed experimentally by Serby [18] and two potential coupling mechanism will be presented in detail.

1.3.1 Primary acoustic instability

Searby reported four distinct regimes of downward propagating flames in a tube as shown in Fig. 1.4 [18]: (I) a curved flame just after ignition without acoustic sound, (II) Primary acoustic instability with a flat flame, (III) corrugated pulsating flame with secondary acoustic instability, and (IV) transition complete turbulent motion. These four regimes of flame behavior can be explained associated with pressure record and flame position as a function of time in Fig. 1.5. For curved flame (Regime I), growth of pressure amplitude is not observed. Thence the acoustic

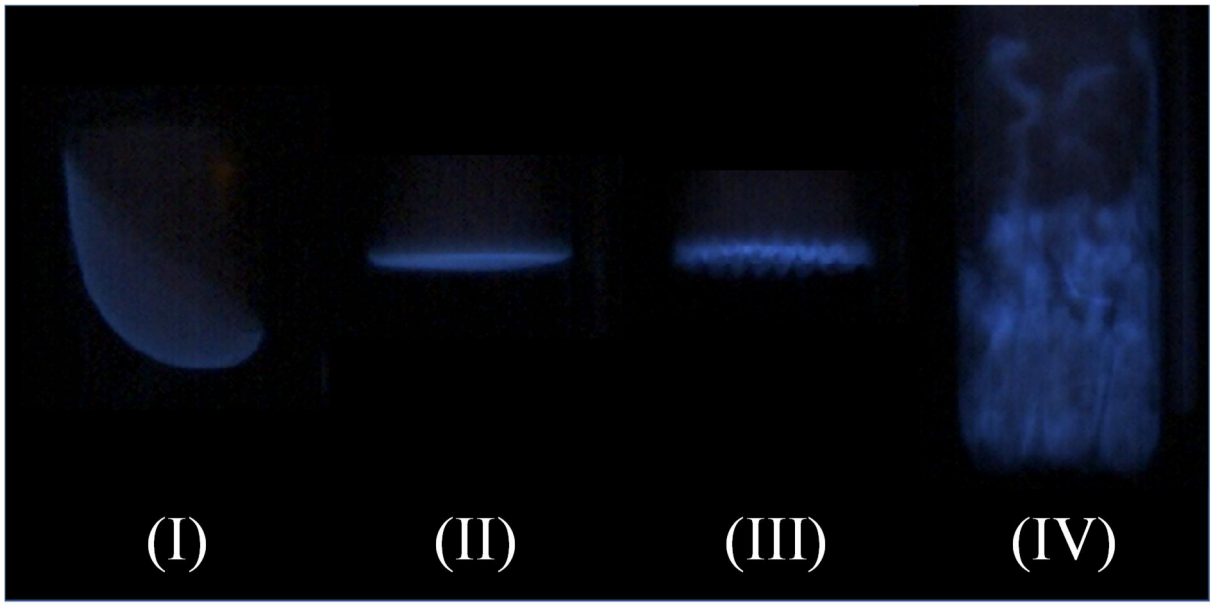

Fig. 1.4 Representative flame shapes under acoustic influences. (I) curved flame, (II) flat flame, (III) corrugated flame and (IV) turbulent flame.

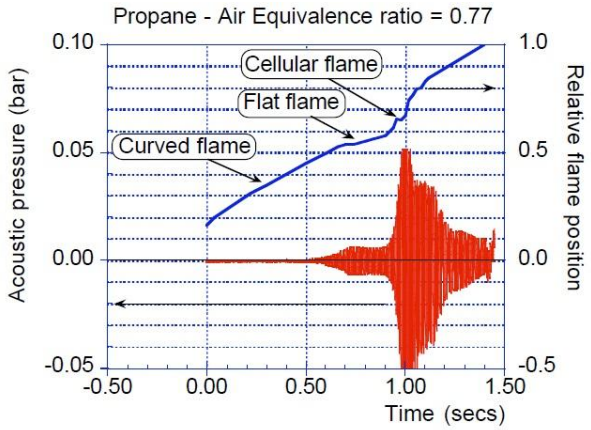

Fig. 1.5 Pressure record of acoustic instability of a premixed propane-air flame propagating in a tube in Ref. [18].

pressure increases and the vibrating flat flame appears as typical feature of the primary acoustic instability.

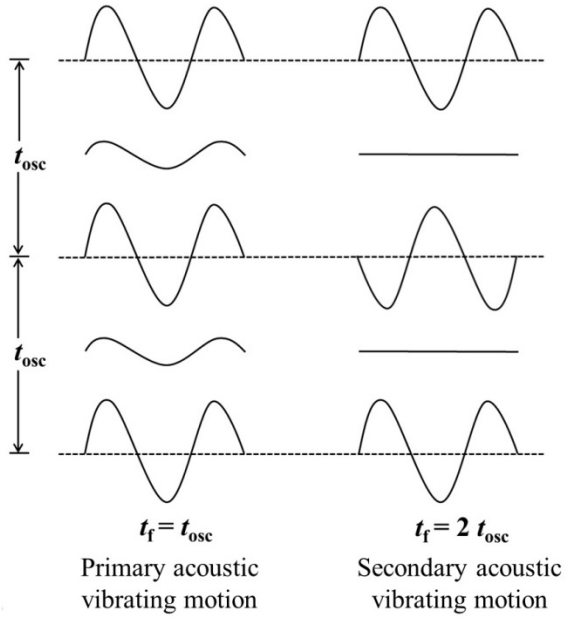

Fig. 1.6 Flame behaviors induced by primary and secondary acoustic instabilities in Ref. [15].

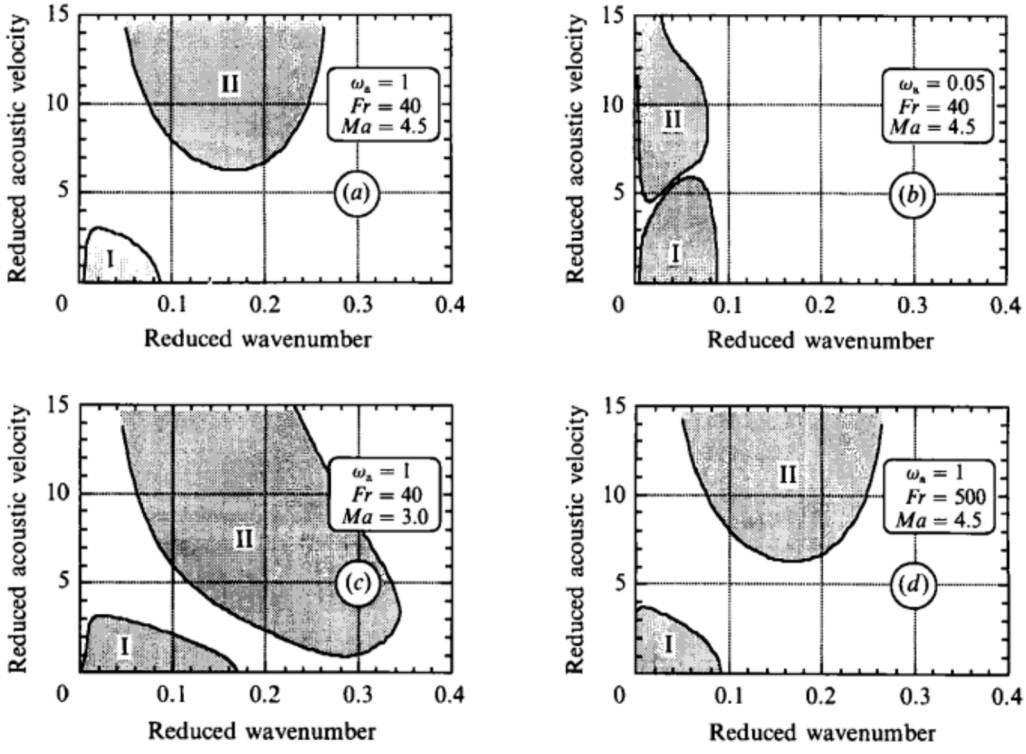

Fig. 1.7 Regions of stability and instability of a periodic acoustic acceleration in Ref. [16].

1.3.2 Secondary acoustic instability

The oscillation of corrugated structure flame has a period that is twice the acoustic period as shown in Fig. 1.6. It is first reported by Markstein [15] and suggested that this parametric instability is induced by a time dependent modulation of the restoring force by diffusive-thermal stabilizing effect for strong acoustic acceleration.

Figure 1.6 shows the stability diagram of acoustic instabilities in the plane of reduced acoustic velocity, U_a/S_L, and reduced wave number, $2\pi d/\lambda$. The lower region (I) at small reduced wave number and low reduced acoustic velocity corresponds to the D-L instability and black region is the primary acoustic instability. The upper region (II) with larger acoustic level is subject to the secondary acoustic instability. As shown in Fig. 1.7, the generation of secondary acoustic instability requires the strong pre-existing finite-amplitude of the primary oscillation.

1.3.3 Coupling mechanisms

Many researchers have investigated to explain the flame-acoustics coupling. In this Section, two potential candidates of coupling mechanism, pressure coupling [10, 15] and acceleration coupling [17, 19], will be introduced.

Dunlap [10] theoretically showed that the local flame heat release rates can be modulated if the pressure and adiabatic temperature of an incoming acoustic wave are in phase. Clavin et al. [15] reported that a total growth rate is proportional to coupling constant, βM, where small Mach number and sufficient long residential time are given. The flame may overcome the damping mechanism due to heat transfer and viscous friction at the tube wall and to acoustic radiation losses at the open end of the tube when the coupling constant is adequately large.

For the generation of primary acoustic instability at propagating in tube, the pressure coupling can be derived. The time derivative of the total energy per unit cross-sectional area, dε/dt, is given as follows.

$$\frac{d\varepsilon}{dt} = \delta P(\delta u_b - \delta u_u) \tag{1-8}$$

Here δP is the pressure fluctuation, δu is the velocity fluctuation and the subscripts u and b identify unburned and burned mixtures, respectively. For the pressure jump across the flame, it is of order ρU^2, where ρ is the density and U is the flame velocity, and it is much smaller than the variations in the acoustic wave, ρc^2, where c is the speed of sound. Thus, it can be supposed that pressures are equal on both sides of the flame. Considering Rayleigh criteria, the problem of key point is how dose $(\delta u_\mathrm{b} - \delta u_\mathrm{u})$ connect to δP in phase. Because, the gas expansion, $(\delta u_\mathrm{b} - \delta u_\mathrm{u})$, is proportional to the fluctuation of the rate of heat release per unit cross-sectional area, δq.

For simplicity of calculation, a one-step reaction with large activation energy is assumed and the chemical reaction occurs in a thin region since the inverse of β implies an effective dimensionless width of the reaction zone [20]. In the present work, Zel'dovich number can be calculated [31] as follows:

$$\beta = E(T_\mathrm{b} - T_\mathrm{u})/(RT_\mathrm{b}^2). \tag{1-9}$$

Peters and Williams [32] define the activation energy, E, as follows:

$$\frac{E}{R} = -\frac{\mathrm{d}2[\ln(\rho_\mathrm{u} S_\mathrm{L})]}{\mathrm{d}(1/T_\mathrm{b})}. \tag{1-10}$$

A small relative variation in the flame temperature induces a modification to the laminar flame velocity, S_L, and the heat flux, q, of order unity:

$$\frac{\delta T_\mathrm{b}}{T_\mathrm{b}} = O(\frac{1}{\beta}) \Longrightarrow \frac{\delta S_\mathrm{L}}{S_\mathrm{L}} = O(1) \text{ and } \frac{\delta q}{q} = O(1). \tag{1-11}$$

In the conservation equation of enthalpy, the relative variation in temperature and pressure in an acoustic wave are of the same order of magnitude:

$$\frac{\delta T}{T} \approx \frac{\delta P}{P} \approx \frac{\rho c \delta u}{P} = M\left(\frac{\delta u}{S_{\mathrm{L}}}\right). \tag{1-12}$$

According to Eq. (1-11), this temperature fluctuation induces a modification of the flame structure and of the heat release of the order $\beta M(\delta u/S_{\mathrm{L}})$. For a relative gas expansion across a discontinuity surface, one may expect the same order of magnitude for the relative velocity jump across the flame to be as follows:

$$\frac{\delta u_{\mathrm{b}} - \delta u_{\mathrm{u}}}{S_{\mathrm{L}}} \approx \beta M\left(\frac{\delta u}{S_{\mathrm{L}}}\right). \tag{1-13}$$

The energy per unit cross-sectional area, ε, which is stored in the acoustic mode of the tube, is of order $(\tau_{\mathrm{a}}\delta u \delta P)$. Therefore, the characteristic order of magnitude of the growth rate of such an acoustic instability, $1/\tau_{\mathrm{ins}} \equiv \varepsilon^{-1}\,\partial\varepsilon/\,\partial t$, according to (1-8) and (1-13) would be the following:

$$\frac{1}{\tau_{\mathrm{ins}}} \approx \frac{\beta M}{\tau_{\mathrm{a}}}. \tag{1-14}$$

Thus, the growth rate of the acoustic instability of planar flames is proportional to the coupling constant, βM.

Now we consider acceleration coupling. Pelcé and Rochwerger [17] introduced a new transfer function defined as follows:

$$Tr = \frac{(\delta u_{\mathrm{b}} - \delta u_{\mathrm{u}})}{\delta u_{\mathrm{u}}}. \tag{1-15}$$

When the mass conservation equation crossing the flame is considered, the amplitude of the outgoing wave in the burned mixture is determined by the following relation:

$$\delta u_{\mathrm{b}} - \delta u_{\mathrm{u}} = \left(\frac{\rho_{\mathrm{u}}}{\rho_{\mathrm{b}}} - 1\right) S_{\mathrm{L}} \delta S \tag{1-16}$$

where δS is the perturbation of the normalized flame area. Thus, the growth rate of the acoustic

instability of curved flames is proportional to $(ak)^2$ because of the relation $S = 1 + \frac{1}{4}(ak)^2$ [17].

1.4 Objective of present research

1.4.1 Motivation

Many studies have been conducted to investigate the thermal acoustic instability. In the experimental studies, experiments involving a propagating flame in a tube are among the most elementary and widely employed types of experiments.

The representative behaviors of a downward-propagating flame in a tube were reported by Serby [18]. Searby and Rochweger studied the above phenomena experimentally and theoretically and reported stability diagrams of the thermo-acoustic instabilities of a downward-propagating flame in a tube [16].

Tsuchmoto et al. conducted the experiment on an upward-propagating flame in a tube to investigate oscillation phenomena with a CO_2 laser method [21]. They controlled the freely propagating flame front by using CO_2 laser irradiation method and it was found that the intentionally-controlled flame front structure could modify the flame propagation behavior, and

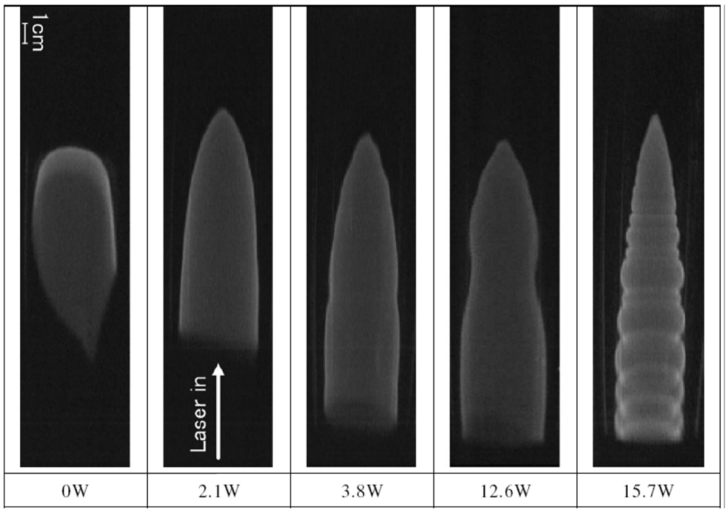

Fig. 1.8 Still images of propagating ethylene-air premixed flames (Le<1) with various applied laser powers in Ref. [21]

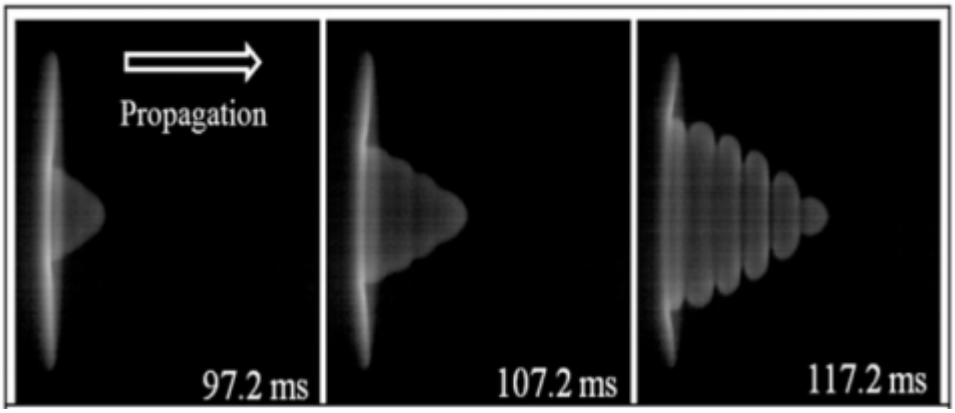

Fig. 1.9 Still image of transient flame motion with laser power 18W in Ref. [23]

it could induce unstable motion of flame front as shown in Fig. 1.8. The external laser irradiation preheats the unburned mixture locally in front of the reaction zone, and the flame propagation velocity increases locally, and here the flame front acquires a strongly curved shape.

Park et al. investigated the transition process of the downward propagating flame of ethylene premixed flame in a tube from the primary acoustic instability to the secondary acoustic instability [22]. They also adapted the CO_2 laser method to control the initiation of the transition process. It was found that a unique structure (ice cream shape) is formed under the presence of acoustic field as shown in Fig. 1.9. They suggested the physical model of the transition process and if a flame tip grows extremely fast, it can result in the enhanced acoustic amplitude to reach the secondary acoustic instability regime. Taniyama et al. conducted experimental research to investigate the process of the transition from the convex disturbed flame structure to the corrugated flame. They also showed the process of the transition in great detail with various laser parameters. Advanced physical mechanism of the transition is proposed by considering the interaction between acoustic wave and deformed flame. Meanwhile, K. Aguilar et al. observed appearance of the concave structure of upward motion

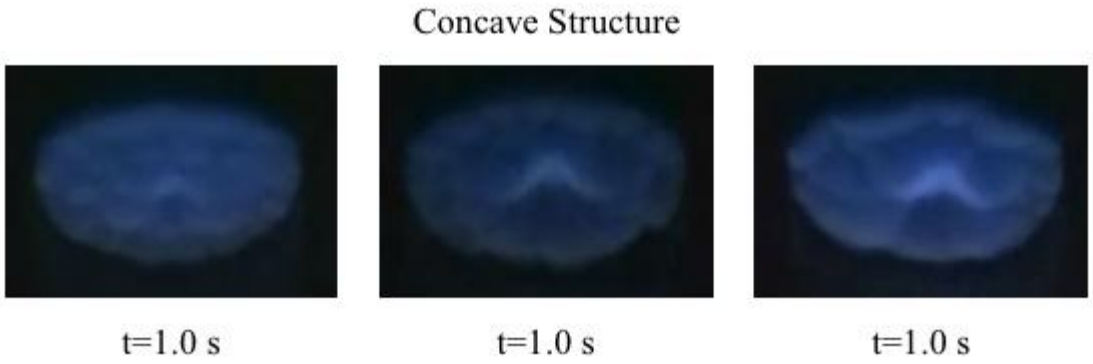

Fig. 1.10. The image of concave structure produced by buoyancy effect in Ref. [24].

of the flow produced by buoyancy effect, not only the convex flame front shape induced by CO_2 laser method as shown in Fig. 1.10 [24]. Although the CO_2 laser irradiation method can produce both convex and concave flame front structure, the above results were under the condition that $Le<1$. Especially, the study on the effects of Lewis number on acoustic instability have rarely been conducted. Because typical feature of primary acoustic instability region is a flat flame, the Lewis number effect attributed to the flame front curvature is very hard to be observed.

The objective of this research is to figure out the Lewis number effect on acoustic instability through controlling flame front shape using CO_2 laser irradiation method.

1.4.2 Scope of present research

In this thesis, first, we report the flame propagating behaviors having artificially controlled flame front shape by CO_2 laser method. The laser irradiation into the unburned mixture deforms the flame shape, resulting in a convex structure, and then the concave structure of the flame front was formed owing to buoyancy induced flow. We examine the acoustic pressure change under various laser irradiation conditions and Lewis number.

Observation of the transition phenomena caused by laser irradiation from primary acoustic instability to secondary acoustic instability will be presented. With highly-resolved images by high speed camera, we could visualize behaviors of the flame propagation and transition behaviors. Two distinct transition behaviors will be presented.

We obtained stability map of transition criteria variation induced CO_2 laser method with various Le in terms of laser power and irradiation time. An attempt was made to evaluate the Lewis number effect quantitatively attributed to flame front curvature. Then quantitative Lewis number effect will be presented.

Chapter 2: Experimental setup

The experimental apparatus is schematically outlined in Fig. 2.1. The propagation tube (transparent acrylic tube, 50-mm inner diameter and 711-mm length) is fixed vertically and charged with the tested gas at atmospheric pressure. To artificially change the flame area, the CO_2 laser-irradiation method is utilized. Ethylene gas plays an important role as the main absorption medium of CO_2 laser light according to the NIST chemical database [25]. The CO_2 laser beam (beam diameter: 3.3 mm, SYNRAD Firestar v20, wave length: 10.6 μm) vertically passes along the center of the tube. The specification of CO_2 laser is shown in Table 2.1. A point ignition system using a spark plug is located near the upper end of the tube. When the spark igniter is activated, the top lid (see, Fig. 2.2) is simultaneously opened by an automatic opening system of the top lid of the tube powered by an electromagnet and a mechanical spring. The direct photo of optical setup is illustrated in Fig.2.3. The focusing lenses (OPHIR DURA-LENS) are made of Zinc Selenide (ZnSe) with an anti-reflective coating. In order to ensure parallel laser beam, it is crucial to set exact optical arrangement. The focusing lenses are

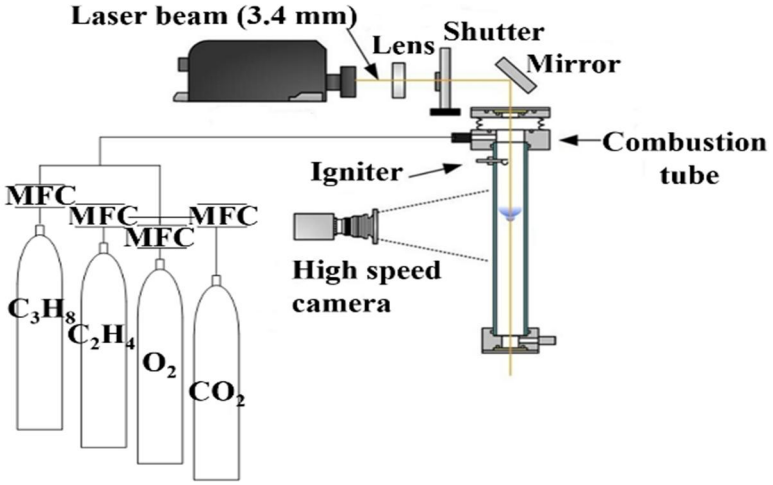

Fig. 2.1 Schematic drawing of the experimental setup.

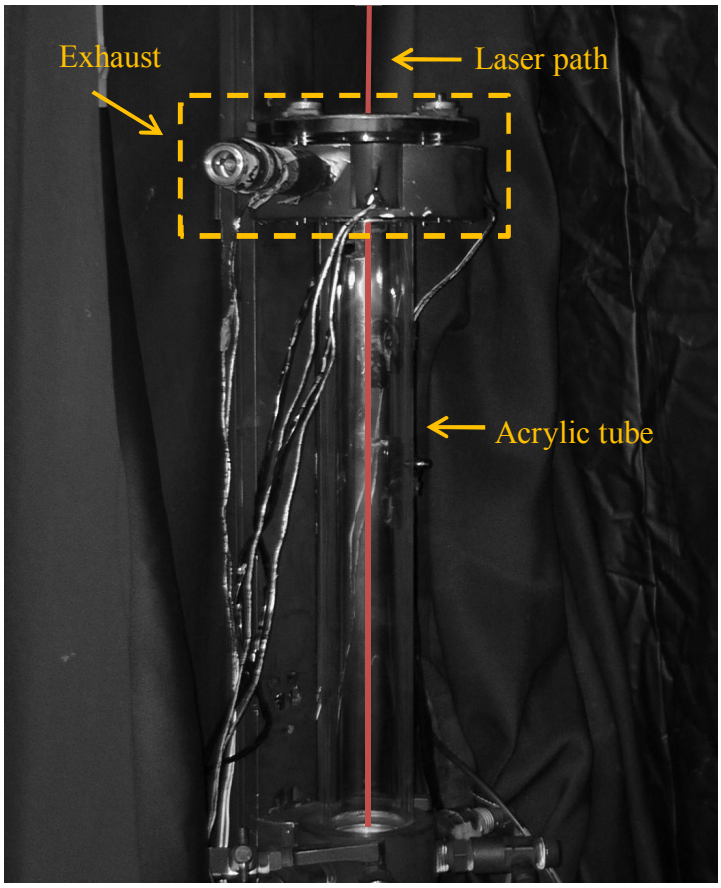

Fig. 2.2 Direct photo of propagation tube.

Table 2. 1 Specification of CO_2 laser.

Model	SYNRAD firestar v20
Wavelength	10.57 ~ 10.63μm
Output Power	20W
Power Stability	±5% (cold start) ±3% (After 2 minutes)
Beam Diameter	2.0mm±0.5mm
Beam Divergence	<7.0mRad
Rise Time	< 100μsec
Ellipticity	<1.2

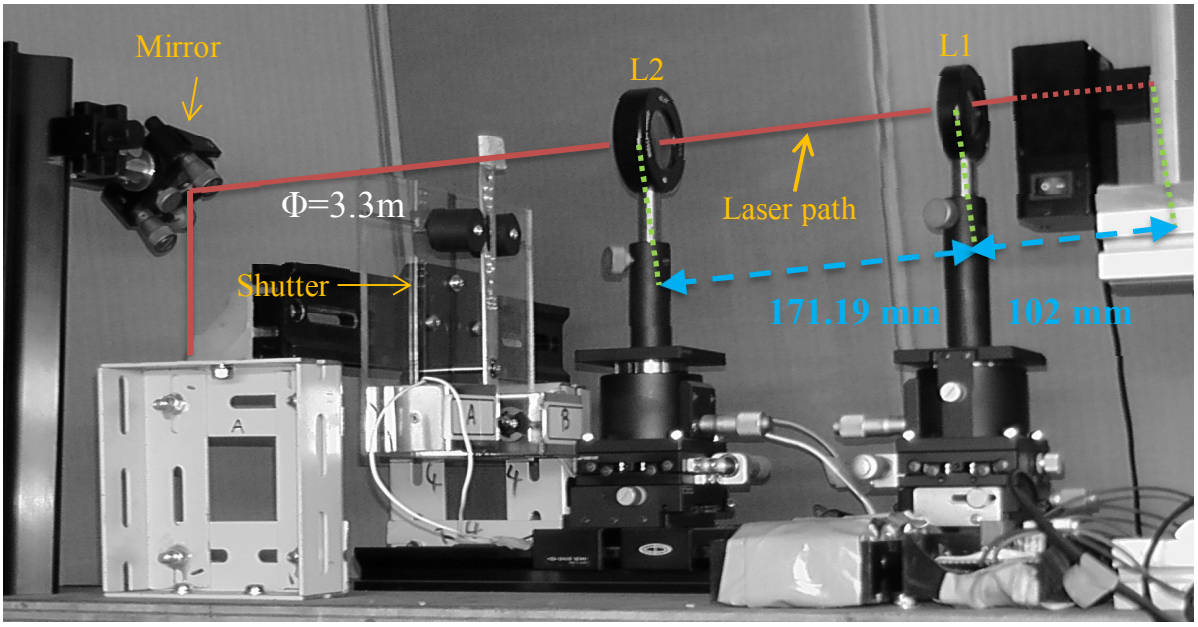

Fig. 2.3 Direct photo of optical setup.

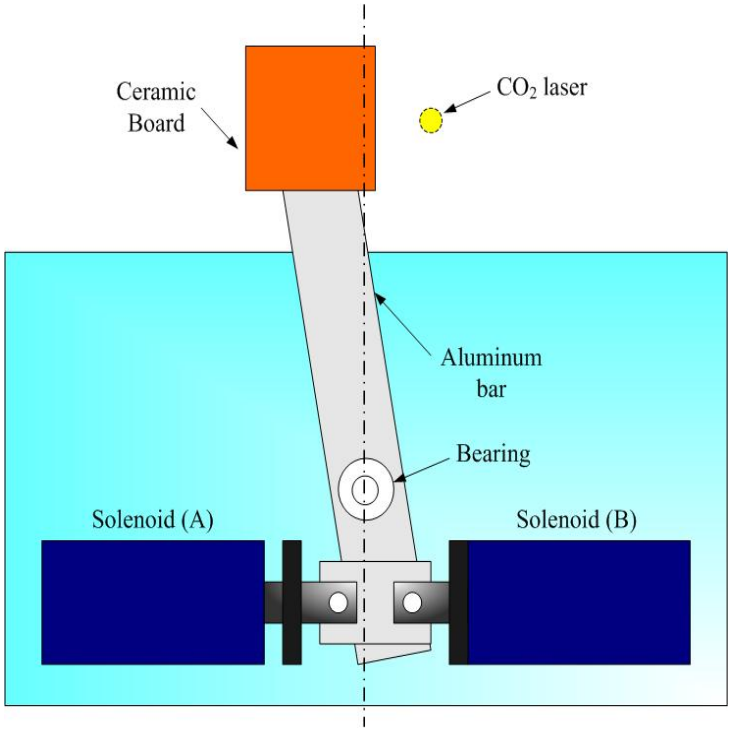

Fig. 2.4 Schematic diagram of mechanical shutter.

Meniscus (L1, focusing length: 63.5 mm) and Plano-Convex (L2, focusing length: 95.25 mm) as shown in Fig.2.3. Mechanical shutter is set in the laser path to control the exposure time and onset time of laser beam. Fig.2.4. depicts the schematic outline of mechanical shutter. To control the exposure time of CO_2 laser, the ceramic board as a shutter (powered by two solenoids) closes and opens according to expected time sequence.

The time-dependent behaviors of the downward-propagating flame are recorded by high-speed cameras. The high-speed camera (nac HSV-500C[3] recording at 500 fps) captures whole images of the propagating flames in the tube. Pressure temporal variation is measured with a PCB Piezotronics 106B52 dynamic pressure sensor located at the bottom end of the tube at a sampling rate of 10 kHz. System sequence is controlled by the programmable controller (MITSUBISHI, FX_0-20MR). The time schedule of the system sequence for continuous laser beam is shown in Fig. 2.5. The onset of the laser exposure is defined as $t = 0.0$ s in the present study.

Chapter 3: Effect of Lewis number on acoustic pressure

In Chapter 3 to examine effect of Lewis number on acoustic instability, the premixed gas composed of ethylene, oxygen, carbon dioxide is set at atmospheric pressure in the tube. Various gas compositions are tested in association with different Lewis number as show in Table 3.1. The laminar burning velocities are calculated using CHEMKIN (Premix code/ USC II) [26]. Comparison of Mix. 1, 2 and 3 provide information on the effect of Lewis number on acoustic instability.

3.1 Flame propagation behaviors with external laser irradiation

Fig. 3.1 shows the flame propagating behaviors under various beginning timing of laser irradiation. The beginning of laser irradiation is defined as 0.0 s. Once the flame was exposed to the external laser beam, the ethylene gas in the gas mixture absorbed laser energy, and subsequently, the preheated unburned mixture may have increased the local flame velocity. Then, the flame front structure deformed, as shown in Fig. 3.1. The convex curvature toward

Table. 3.1 The tested gas and laser irradiation condition in Chapter 3.

Mixture	C_2H_4 [%]	O_2 [%]	CO_2 [%]	Φ	S_L	Le
1	0.054475	0.20428	0.741245	0.8	10.03831	1.05
2	0.057483	0.215563	0.726954	0.8	12.50907	
3	0.074562	0.186405	0.739033	1.2	9.986134	0.79
	Laser power (W)	0 ~ 18 W		Laser irradiation timing	+ 0.7, +1.1, +1.5 from ingnition	

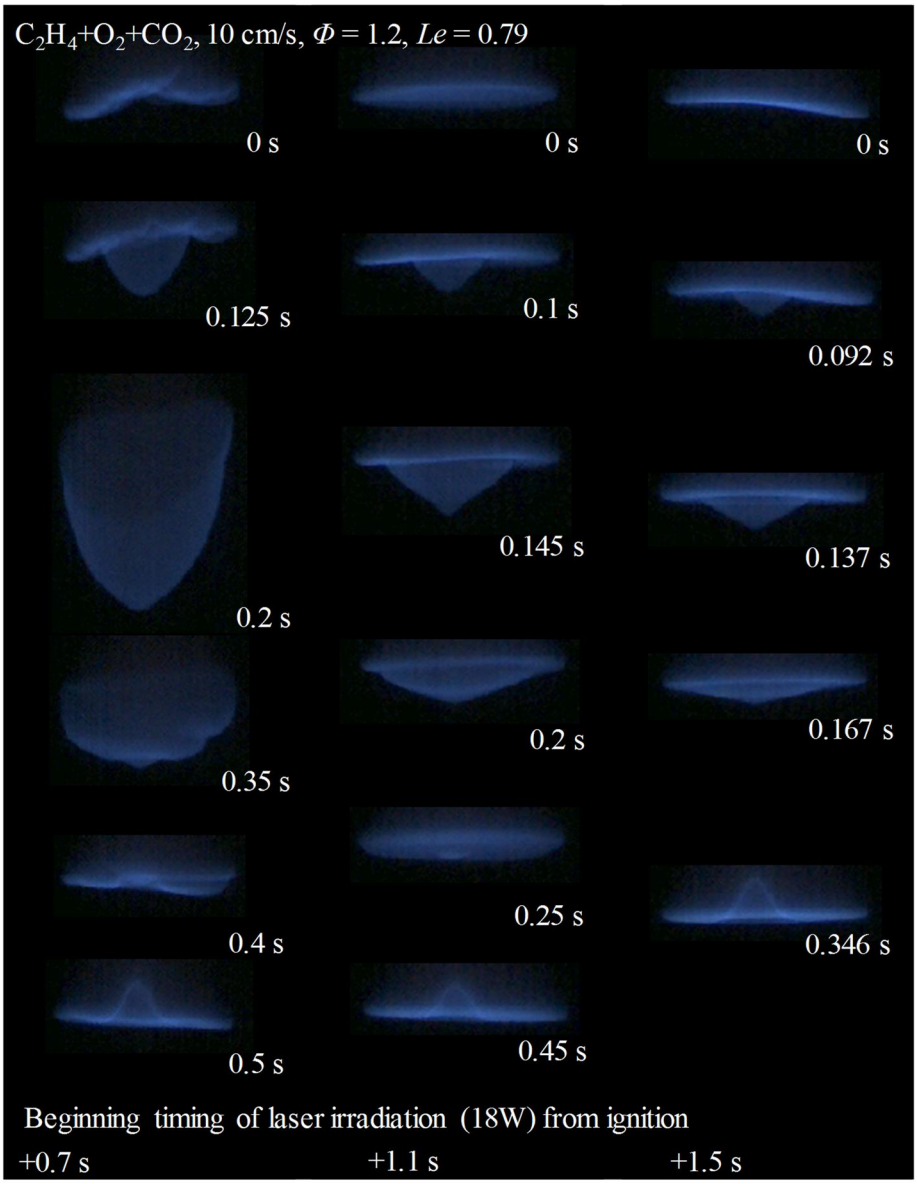

Fig. 3.1 The flame propagation behaviors with various laser irradiation conditions.

unburned mixture was generated immediately after laser exposure, and then the concave curvature of the flame front was formed induced by buoyancy flow. The convex curvature artificially controlled by laser irradiation decreases when the beginning of laser irradiation is getting delayed. In Fig. 3.2, acoustic pressure change at the bottom of the tube as a function of

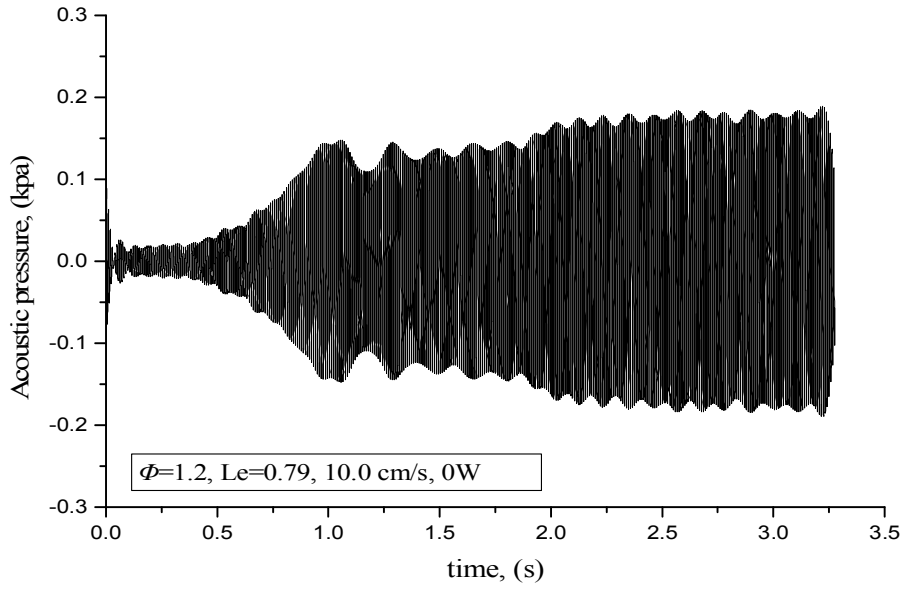

Fig. 3.2 Acoustic pressure at the bottom of the tube as a function of time in Mix. 3.

time is presented without laser irradiation. The growth of pressure amplitude starts from 0.5s and the acoustic pressure is fully saturated at about 2.0s. Once acoustic pressure is saturated in primary acoustic region, the vibrating flat flame maintains its shape. It means that the hydrodynamic perturbation is suppressed by primary acoustic instability. By same reasoning as the above, the deformation due to laser irradiation is inhibited by primary acoustic instability. The growth of flame surface area can result in enhanced acoustic amplitude and the vibrating curved flame induced by laser irradiation can undergo the diffusive thermal instability. Thus, it is necessary to explore the response of acoustic pressure to the change of flame front shape. This discussion will be presented in Section 3.2.

3.2 Effect of CO_2 laser irradiation on acoustic pressure

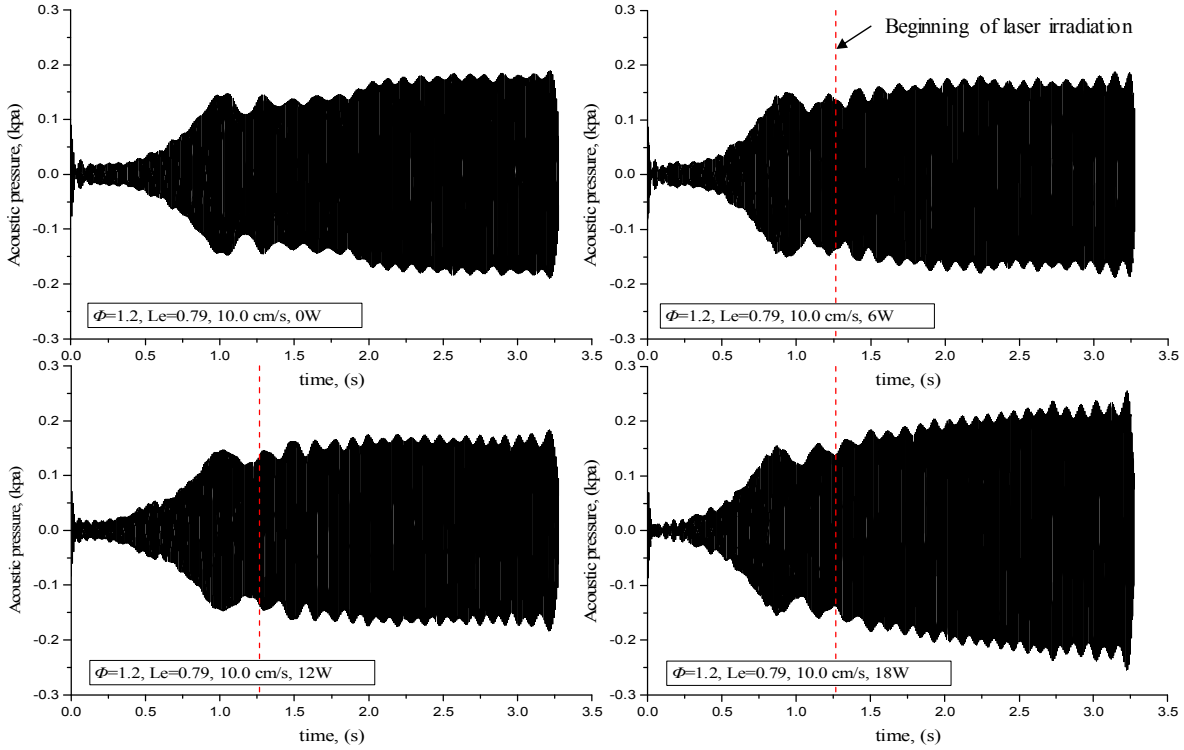

Fig. 3.3 Acoustic pressure with various laser power at the bottom of the tube as function of time in Mix. 3 (+1.5s). (a) 0W, (b) 6W, (c) 12W, (d) 18W.

Fig. 3.3 shows acoustic pressure with various laser power which irradiated at +1.5s from the ignition. Although the laser power is increased up to 18W, the acoustic pressure is almost identical with no laser irradiation condition. When we reconsider the flame surface area change in Fig. 3.1, the growth of flame surface area induced by laser irradiation was very limited owing to primary acoustic instability at which the beginning timing of laser irradiation is +1.5s. Thus, it is necessary to examine acoustic pressure at the condition which laser irradiation is effective to control the flame surface area.

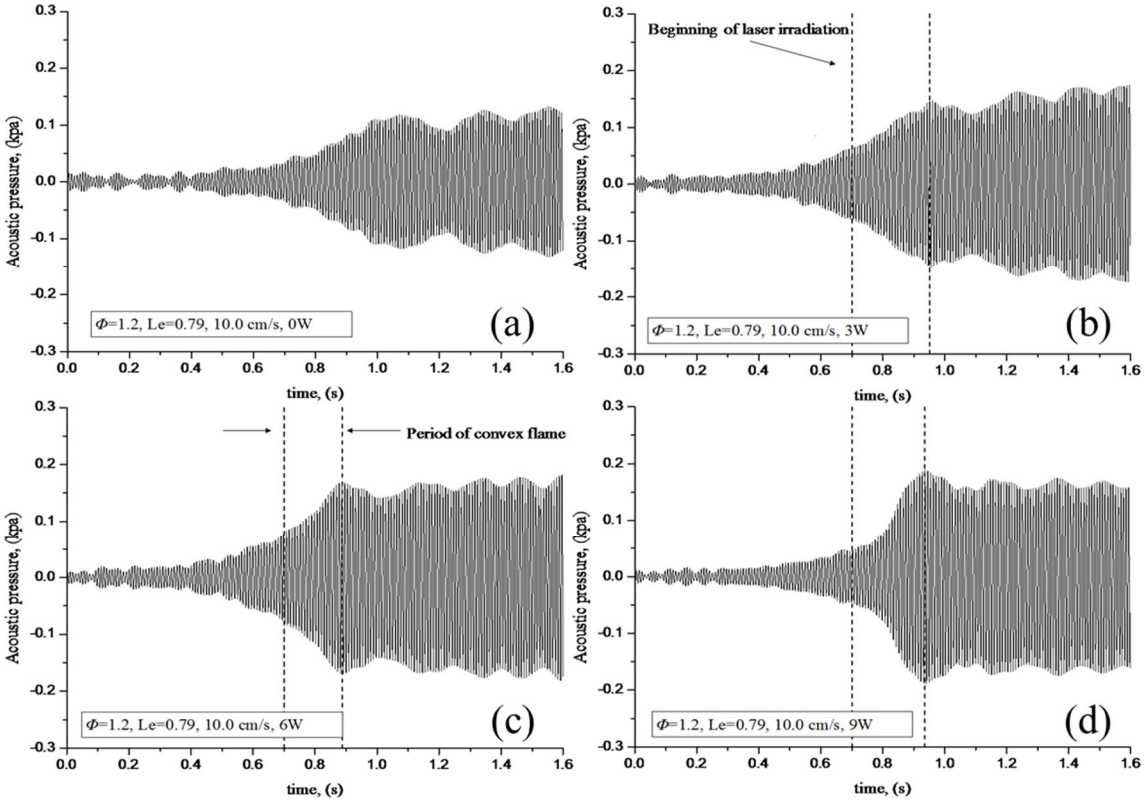

Fig. 3.4 Acoustic pressure with various laser power at the bottom of the tube as function of time in Mix. 3 (+0.7s). (a) 0W, (b) 3W, (c) 6W, (d) 9W.

Fig. 3.4 shows acoustic pressure with various laser power at the bottom of the tube as function of time in Mix. 3 (+0.7s). The growth rate of acoustic pressure at the period that the flame front is convex structure is increased with increasing the laser power (amplitude of curvature). The laser irradiation with higher power can allow relatively larger amplitude of convex structure. It means that the effect of diffusive thermal instability is also getting stronger with increasing laser power. Moreover, in Fig. 3.4, the Lewis number is less than unity (0.79), the mass diffusion process of deficient reactant is more dominant than the heat diffusion. Then the flame temperature is locally increased and it causes that the acoustic pressure amplitude rises.

Fig. 3.5 shows also acoustic pressure with various laser power in terms of time in Mix. 2

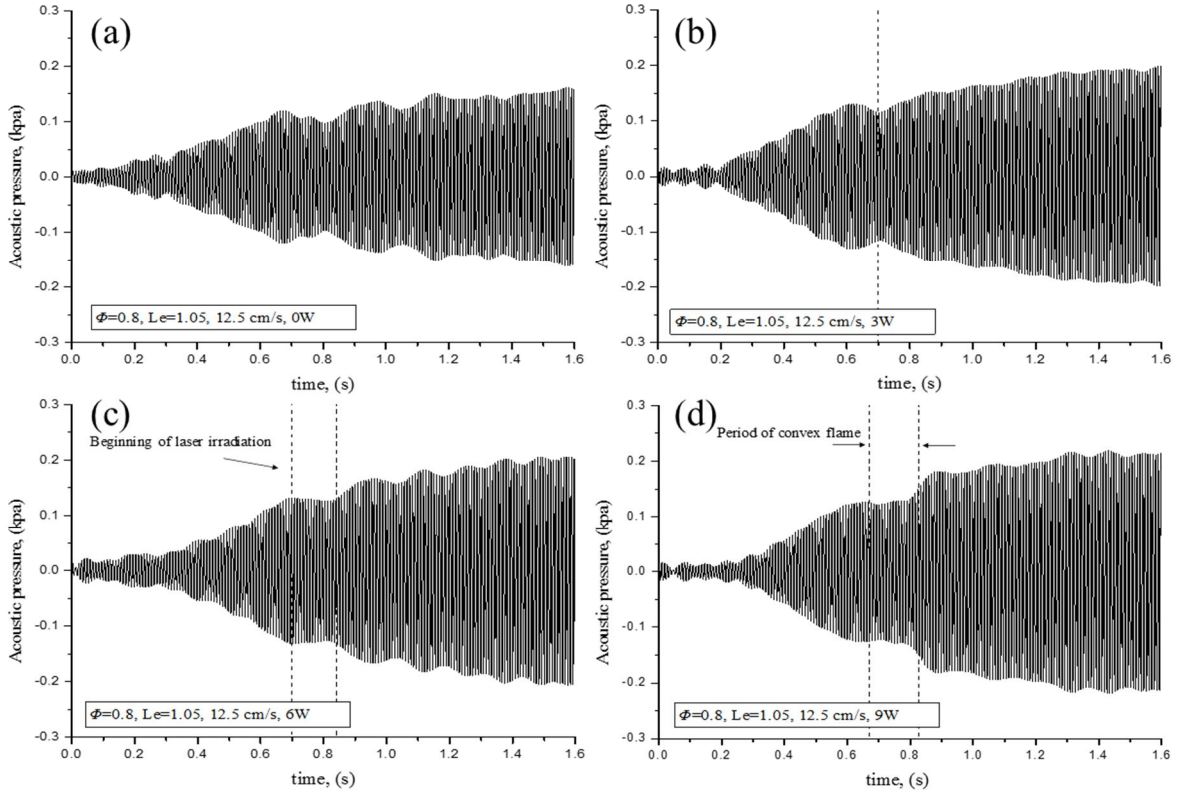

Fig. 3.5 Acoustic pressure with various laser power at the bottom of the tube as function of time in Mix. 2 (+0.7s). (a) 0W, (b) 3W, (c) 6W, (d) 9W.

as a comparison with low Lewis number condition. The convex structure does not appear at Fig. 3.5 (b) because the laser power is not enough strong to induce a sufficient amplitude of convex flame front curvature. With increasing the laser power in Fig. 3.5 (c) and (d), the period of convex flame can be secured. The amplitude of acoustic fluctuation steadily grows until the beginning of laser irradiation. The flame is subsequently transformed into a convex structure. Considering the acoustic pressure fluctuation modification by laser irradiation, the growth of pressure amplitude is suddenly suppressed as shown in Fig. 3.5 (c) and (d). It is completely opposed to the result of Fig 3.4. In the fact that the Lewis number is larger than unity in Fig. 3.5, and therefore, the heat diffusion is more dominant process. It implies that there is the defocusing effect of heat flux and it brings about reducing of flame temperature and the growth

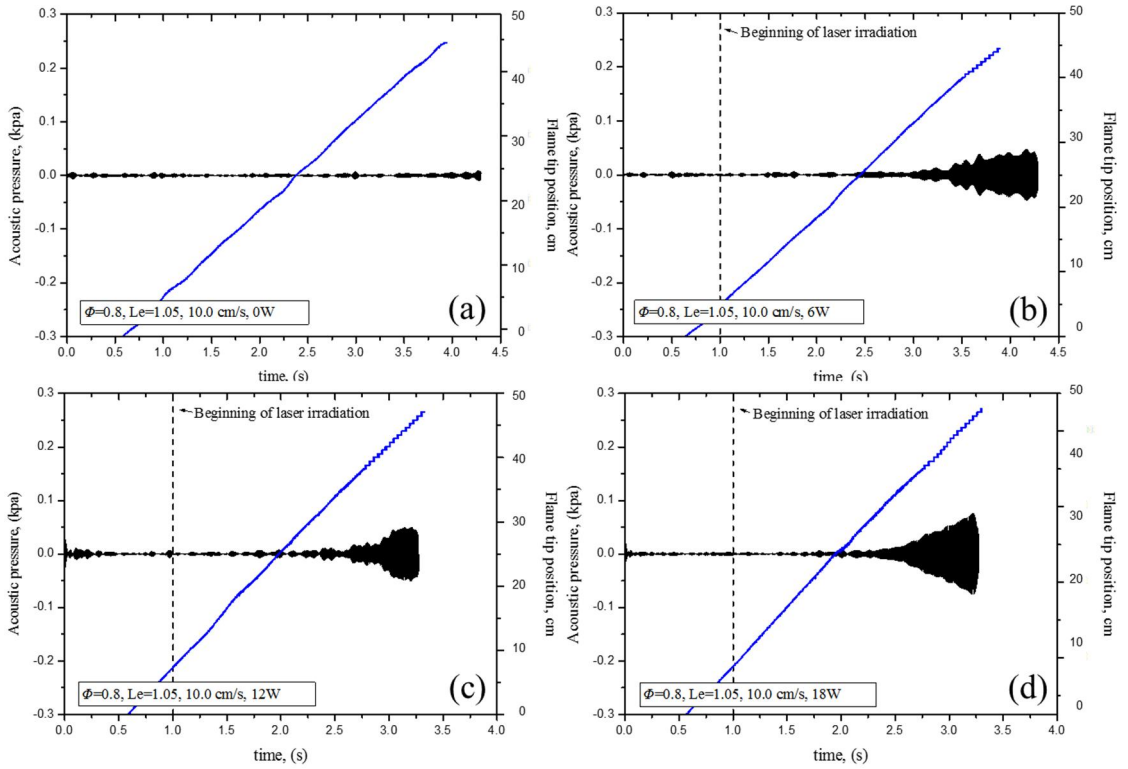

Fig. 3.6 Acoustic pressure at the bottom of the tube as a function of time with various laser power and temporal flame tip position in Mix. 1. (a) 0W, (b) 3W, (c) 6W, (d) 9W.

rate decrease.

Fig. 3.6 shows temporal flame tip position and measured acoustic pressure fluctuation at the bottom of the tube as a function of time in Mix. 1. With no laser irradiation, neither acoustic sound nor acoustic pressure fluctuation is obtained as shown in Fig. 3.6. However, In Fig. 3.6 (a), (b), and (c), the acoustic pressure fluctuation accompanied with the flame oscillation in latter part of the flame propagation. It means that the transition from hydrodynamic instability region (regime I in Fig. 1.6) to primary acoustic instability region (black space in Fig. 1.6) takes place. In latter part of flame propagation which the growth of acoustic pressure appears, the concave structure by buoyancy-induced flow exists only. The flame temperature tends to be raised attributed to convergence of heat flux with concave structure in the condition that the

Lewis number is larger than unity. Summarizing the above experimental observation, the importance of diffusive thermal effect on the acoustic instability can be pointed out: (1) the growth rate of acoustic pressure is raised with increasing the laser power for Le<1 because the convex curvature has a focusing effect on the concentration of the deficient reactant approaching the flame, (2) the growth of acoustic pressure is suddenly suppressed during the period of convex structure for Le>1. It also can be elucidated by the mechanism of mass-thermal diffusion, and (3) the transition from hydrodynamic instability region to primary acoustic instability region is happened.

3.3 Effect of perturbation of flame surface area on growth rate of primary acoustic instability

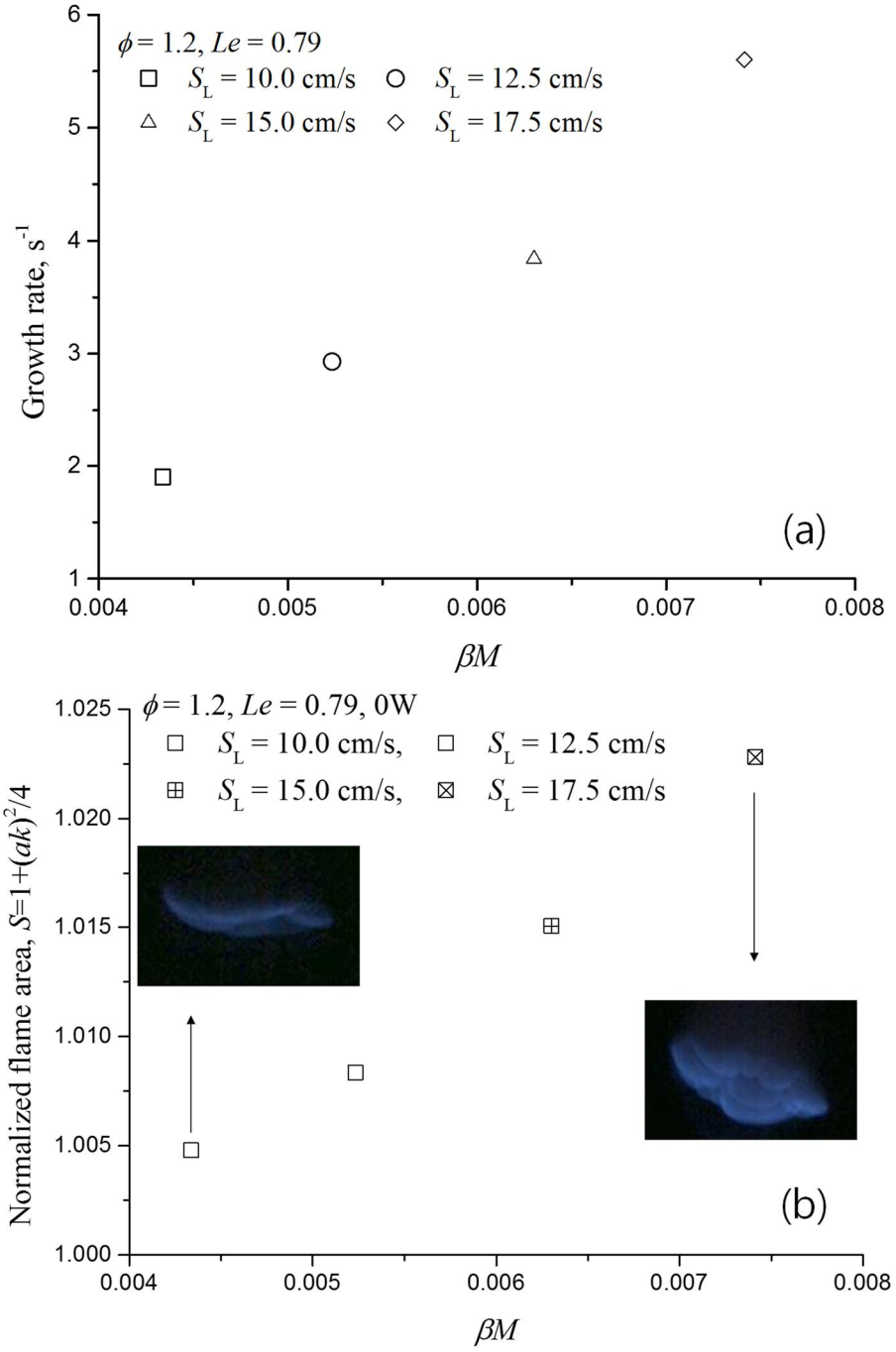

Fig. 3.7 (a) The growth rate variation along coupling constant (βM) (b) Normalized flame area variation with coupling constant (βM).

Figure 3. 10 shows that the growth rate and normalized flame area variation with various coupling constant, βM. The coupling constant was proportional to the growth rates as shown in Fig. 3. 10 (a). According to mechanism of pressure coupling, the growth rate is proportional to coupling constant, βM. Clavin and Pelce reported [10] that the computed growth rates of acceleration coupling were found to be an order of magnitude higher than that of pressure coupling mechanism. In fact, the growth rate caused by pressure coupling turned out to be of the order of 0.1, however, the growth rate of experimental data is of the order of 1. Note that the growth rate is also proportional to coupling constant, whereas the flame surface area also increases with coupling constant as show in Fig. 3. 10 (a) and (b). It implies that two important parameters is perturbed with increasing laminar burning velocity (change of gas composition), which are coupling constant (pressure coupling) and the flame surface area (velocity coupling). In this situation, the perturbation of flame surface area is needed without coupling constant change and the laser irradiation method would be appropriate approach.

In this Section, we would like to confirm that the effect of variation of flame surface area owing to the laser irradiation on the acoustic pressure and its growth rate of primary acoustic instability at fixed coupling constant conditions. Note that the acceleration coupling denotes the normalized flame area is proportional to the growth rate of the acoustic instability of curved flame. Thus, controlling flame surface area could be appropriate approach to secure practical evidence of acceleration coupling.

Figure 3.8 shows acoustic pressure variation with various beginning timing of laser irradiation and flame shapes controlled by laser irradiation for $Le<1$. The flame surface areas decreased as the beginning timing gets later and the growth rate also declined even with same laser power. Especially the flame surface area is much higher for (b) compare to (d) in Fig. 3.8. The growth rate of primary acoustic instability also decreases as the beginning timing is getting

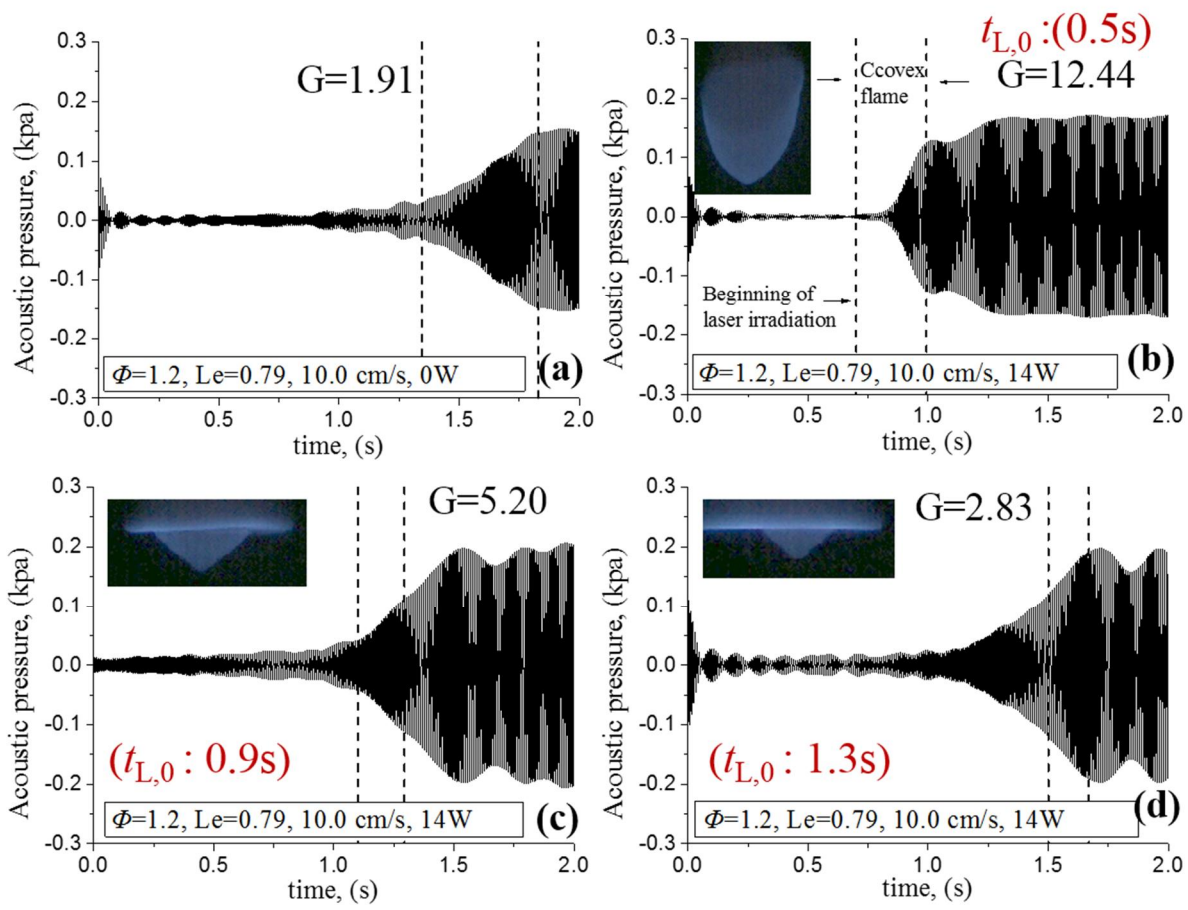

Fig. 3.8 Controlled flame shapes and acoustic pressure with various beginning timing of laser irradiation at the bottom of the tube as function of time for Le<1 (a) 0W (b) 14W, 0.5s, (c) 14W, 0.9s, (d) 14W, 1.3s.

late ($1.90s^{-1}$ ~ $12.44s^{-1}$). It means that the growth rate is proportional to the flame surface area. The change of beginning timing of laser irradiation also modifies initiation of primary acoustic instability. Earlier laser irradiation makes earlier occurrence of primary acoustic instability (compare (a) and (d)). It means that the flame location is relatively closer to the top of tube at the moment of occurrence of primary acoustic instability. Figure 3.9 shows the growth rate variation along the position of tube. The growth rate dramatically increases along the position of tube until about 0.3. Reconsidering Fig. 3.8, the occurrence of primary acoustic instability

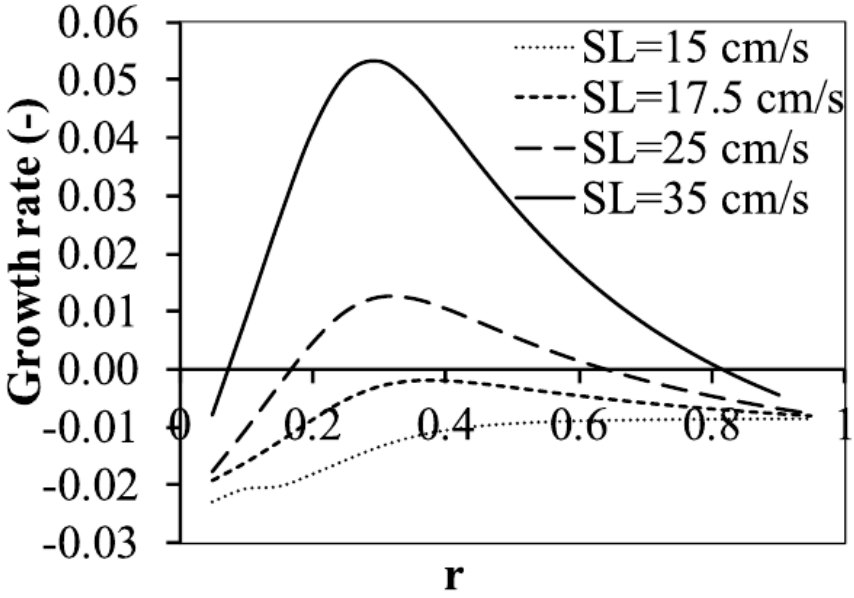

Fig. 3.9 Theoretical growth rate variation along the length of tube for various S_L in Ref. [27]

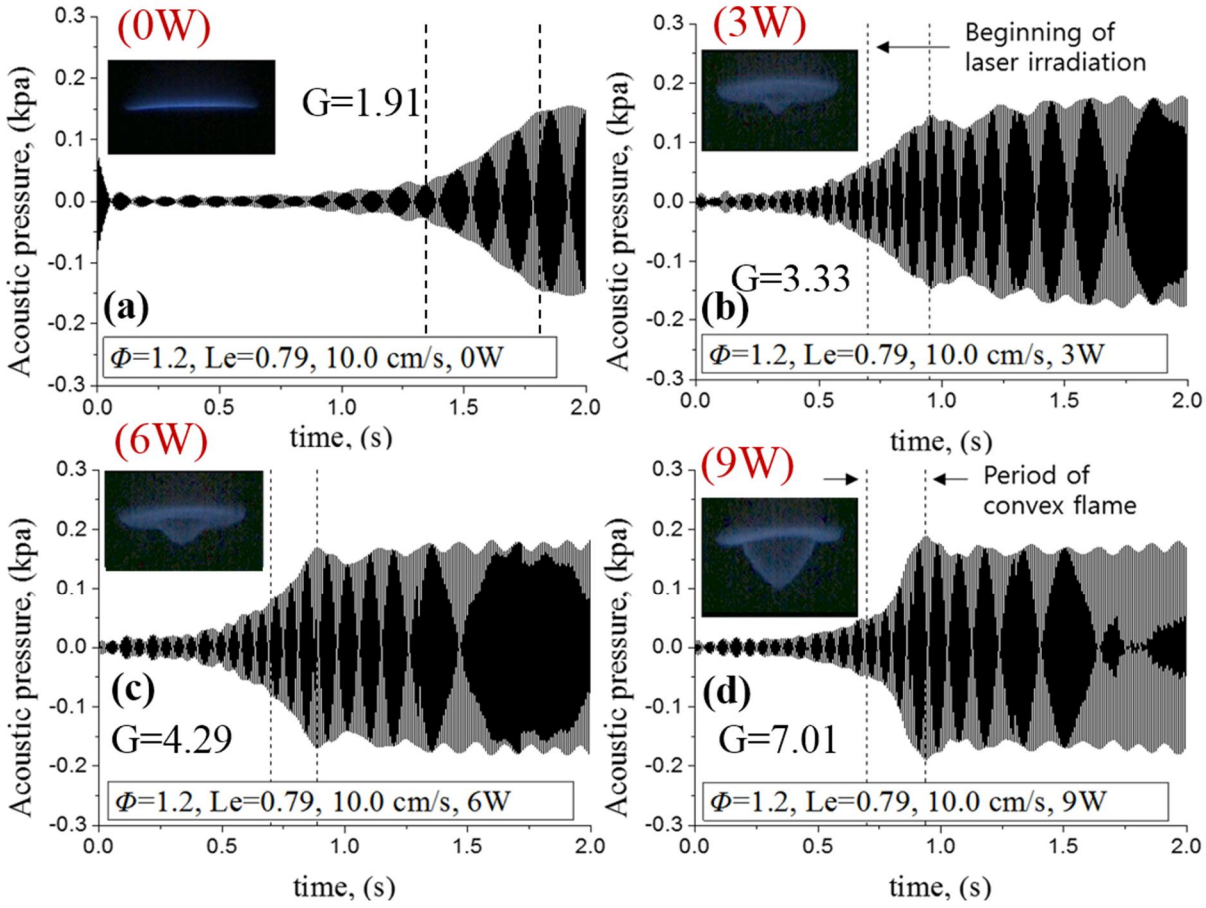

Fig. 3.10 Controlled flame shapes and acoustic pressure with various laser power at the bottom of the tube as function of time for Le<1 (a) 0W, (b) 3W, (c) 6W, (d) 9W.

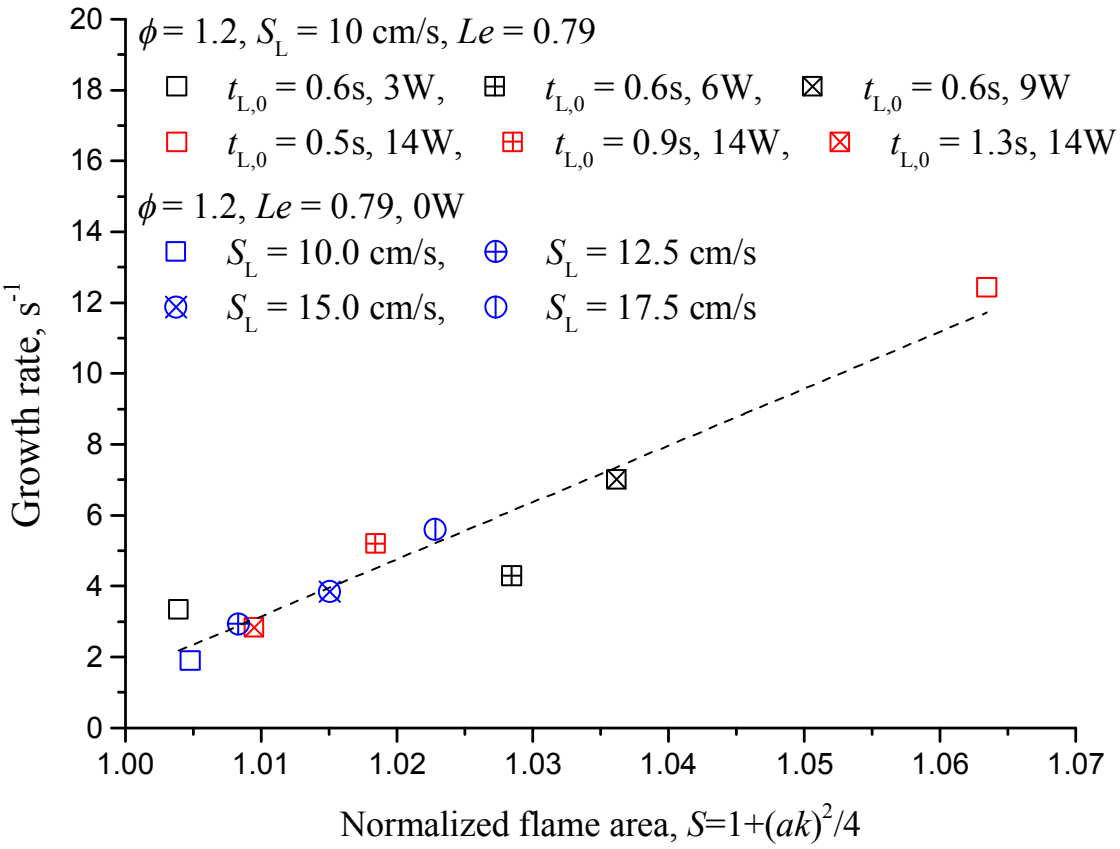

Fig. 3. 11 Growth rates of acoustic pressure as a function of normalized flame area. (Le=0.79)

is earliest at (b) and latest at (d). According to Fig. 3.9, the growth rate should be largest at (d).

However, the largest growth rate was observed at Fig. 3.8 (b). It implies that the various growth rates were determined by the flame surface area change rather than the flame location of tube.

Figure 3.10 shows that controlled flame shapes and acoustic pressure with various laser power at the bottom of the tube as function of time for Le<1. The flame surface area increases with the laser power increases. The growth rate also increases as the flame surface area rise. With above experimental observation, it was confirmed that the growth rate is proportional to the flame surface area. it also implies that the velocity coupling also works as a coupling mechanism of primary acoustic instability.

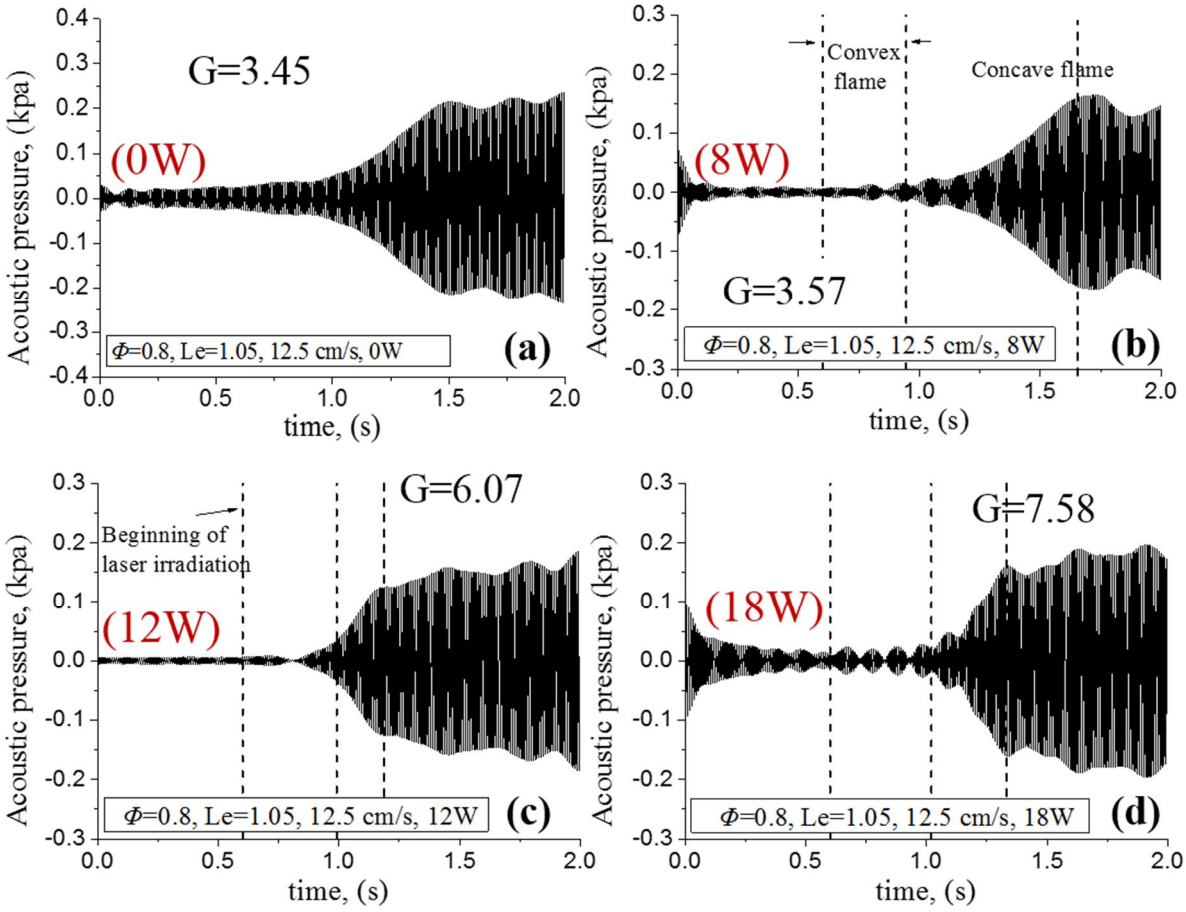

Fig. 3.12 Controlled flame shapes and acoustic pressure with various laser power at the bottom of the tube as function of time for Le>1 (a) 0W, (b) 8W, (c) 12W, (d) 18W.

Bases on above experimental results, the normalized flame area can be obtained and the growth rate variation along the normalized flame area is illustrated in Fig. 3. 11. The linear relationships between the growth rate and normalized flame area was obtained based on experimental results (correlation coefficient = 0.96). The growth rate of initial flat flame (0W) was 1.90 s^{-1} and the it rose to about 6 times (12.44 s^{-1}) where the laser power was 14W, 0.5s. These results clearly demonstrate that the perturbation of the flames area can induce variation of growth rate of acoustic pressure in primary acoustic instability, and therefore, it also implies that the velocity coupling also works as a coupling mechanism of primary acoustic instability.

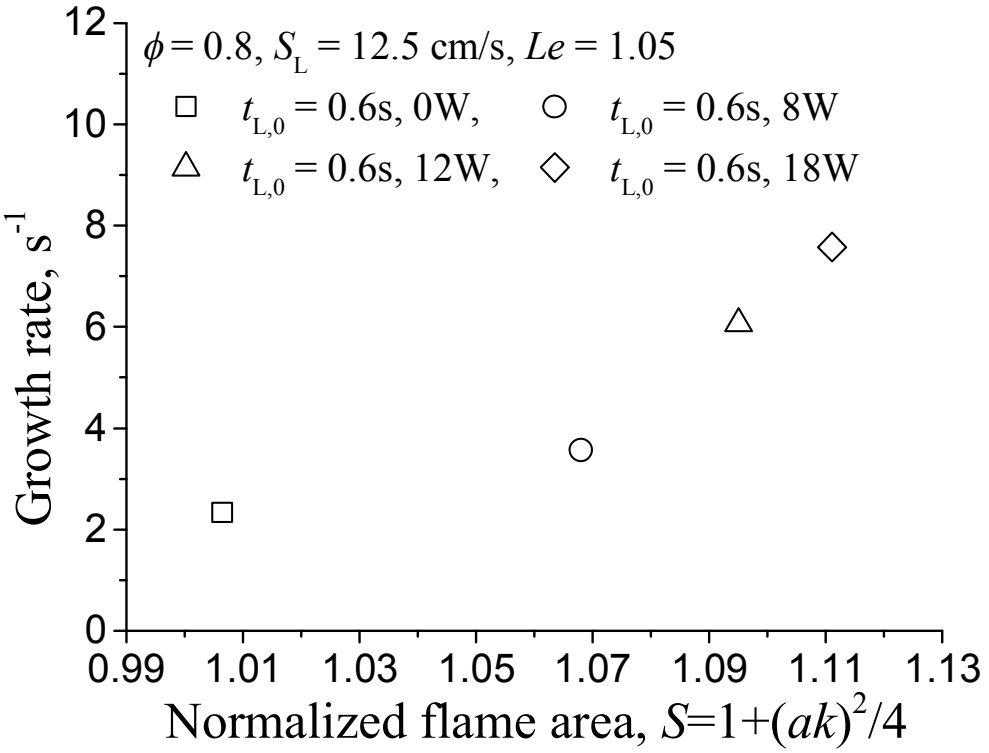

Fig. 3.13 Variation of growth rate of primary acoustic instability with concave flame surface change for *Le*>1.

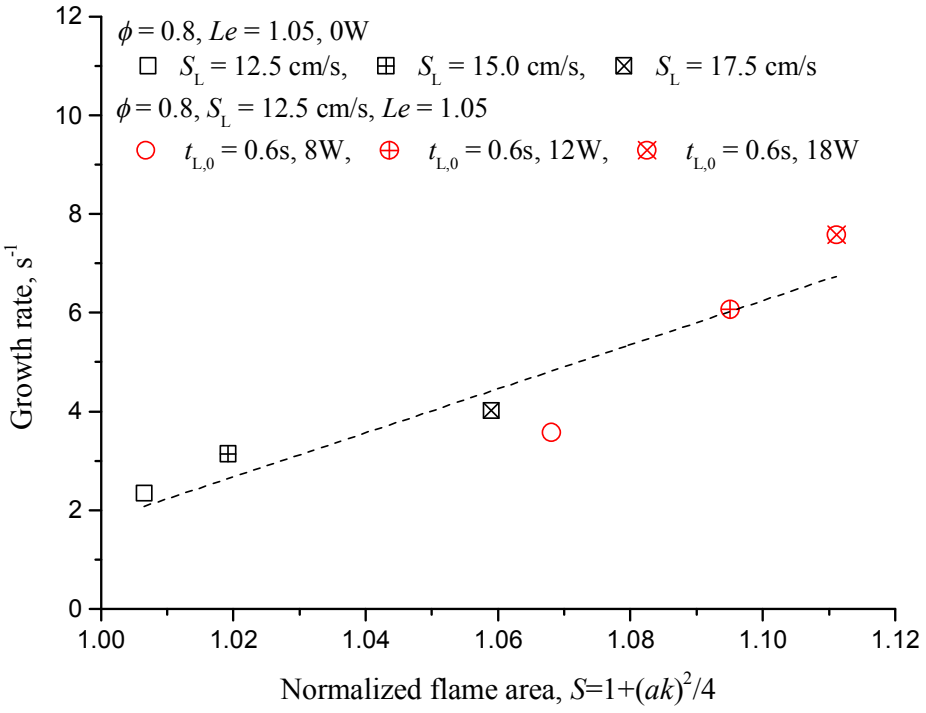

Fig. 3.14 Growth rates of acoustic pressure as a function of normalized flame area. (Le=1.05)

Figure 3.12 shows acoustic pressure change with various laser power for *Le*>1. With laser irradiation, the flame shape is deformed and the convex flame appears first, then the concave flame could be obtained. For all condition, the saturation by primary acoustic instability is not started while the flame is the convex structure, which is conflicting result with *Le*<1. The formation of convex flame in *Le*>1 induces the defocusing effect of heat flux, then the local burning velocity is reduced. Thus, the generation of acoustic instability is suppressed even with the flame surface area increase dramatically. Once the concave flame is formed in *Le*>1, the burning velocity is increased due to the converged thermal diffusion. Finally, the primary acoustic instability is generated with amplified burning intensity owing to *Le* effect.

Figure 3.13 shows that the growth rate change with perturbation of concave flame area induced by laser irradiation. The concave flame area increases with the laser power increase. The growth rate of primary acoustic instability also increases as concave flame area increase. It implies that the growth of acoustic pressure amplitude is not only caused by flame surface area increases but very relevant to the *Le*.

The growth rates with normalized concave flame area at various laser power and laminar burning velocity are summarized at Fig. 3.14. The linear relationship between the growth rate and concave flame area is found. Above experimental observation shows that the growth rate change is well agreement with velocity coupling and the *Le* effect is also sufficient as well.

3.4 Concluding remarks

This Chapter 3 deal with the effect of the Lewis number on acoustic instability of downward-propagating flame in a combustion tube through controlling flame front structure by CO_2 laser irradiation method. The investigation was conducted under two different Lewis number condition. The generation of larger convex curvature by laser irradiation can facilitate the rise of growth rate of acoustic pressure for Le<1, and the focusing effect on the concentration of the deficient reactant approaching the flame contributes to that phenomena. For Le>1, the growth of acoustic pressure is inhibited accompanied with the convex structure. It can be also elucidated by the mechanism of diffusive thermal instability. Contrary to Le<1, the thermal diffusion process is more dominant for Le>1 and hence the defocusing effect of heat flux is relatively stronger than the convergence effect of concentration of the deficient reactant. Therefore, the convex curvature for Le>1 brings about the suppression of growth of acoustic pressure. On the other hand, the concave curvature can be obtained by buoyancy induced flow subsequent to the generation of convex curvature with laser irradiation. Then, the heat flux converges from a large segment of reaction sheet upon diffusion zone. Thus, the flame temperature tends to be raised. The enhanced heat release from flame can amplify the acoustic wave and the transition from hydrodynamic instability region to primary acoustic instability region can be observed.

The flame surface area increased as the laser power rises and beginning of laser irradiation is earlier for $Le<1$. Once the primary acoustic instability occurs, the flame surface area change is suppressed for $Le>1$. For $Le<1$, the growth rate of acoustic pressure increased while the flame has the convex curvature. The growth rate of acoustic pressure increased with increasing flame surface area for $Le<1$. The normalized flame area has linear relationship with the growth rate of acoustic pressure. The growth rate rose through controlling flame surface area up to about 6

times (1.90 to 12.44). In Le>1, the primary acoustic instability is not initiated while the flame is convex structure contrary to in case of Le<1. The growth rate acoustic pressure in Le>1 is increased with increasing concave flame area and the linear relationship is obtained between the growth rate and concave flame area in Le>1. These results can be practical evidence of effect of velocity coupling on acoustic instability and the effect of Le on acoustic instability.

Chapter 4: Effect of Lewis number on transition criteria from primary acoustic instability to secondary acoustic instability.

The object of this Chapter 4 it to examine the effect of Lewis number on transition criteria from the primary to the turbulent flame motion in terms of laser power and exposure time. In Chapter 3, the artificially controlled flame surface structure influences on the acoustic pressure fluctuation. The acoustic amplitude increases with increasing burning intensity. Hence, when the acoustic wave is amplified by controlling flame front curvature, it may be possible to induce the transition from primary acoustic instability to secondary acoustic instability.

In the present chapter, an attempt is made to generate the transition in terms of laser light intensity and elapsed time with continuous laser exposure. Further, the dynamic behaviors of flame propagating behaviors and the stability map of the transition were obtained. We will discuss how the Lewis number works on the acoustic instability and the transition from the primary to the turbulent flame motion.

In the present chapter, the premixed gas mixtures were composed of ethylene, oxygen, carbon dioxide, and propane. The ethylene gas concentration of gas composition mainly influences on laser energy absorption rate based according to the NIST chemical database [25]. Therefore, the ethylene gas is mostly used as a fuel. In some cases, ethylene and propane mixture was used to keep ethylene concentration in the gas composition to attain constant laser absorption rate. The addition of propane also allowed to increase Le up to 1.09, which gives convincing data in the effect of Le. The tested gas mixture information is shown in Table. 1. The combustion velocity in the table are calculated using CHEMKIN (Premixed code/USC II)

Table 4.1 The tested gas information.

C_2H_4 [%]	C_3H_8 [%]	O_2 [%]	CO_2 [%]	Φ	S_L	*Le*
0.06022		0.225825	0.713955	0.8	15	1.05
0.062825		0.235593	0.701583	0.8	17.5	
0.065185		0.244444	0.690371	0.8	20	
0.067414		0.252802	0.679784	0.8	22.5	
0.069512		0.260671	0.669817	0.8	25	
0.074562		0.186405	0.739033	1.2	10	0.79
0.078543		0.196358	0.725098	1.2	12.5	
0.082068		0.205169	0.712763	1.2	15	
0.085385		0.213462	0.701153	1.2	17.5	
0.04	0.0124822	0.228014	0.719504	0.8	12.5	1.09
0.04	0.0146618	0.241636	0.703702	0.8	15	
0.04	0.0163676	0.252298	0.691335	0.8	17.5	
0.04	0.018376	0.26485	0.676774	0.8	20	
0.04	0.0199153	0.274471	0.665614	0.8	22.5	
0.04	0.0268587	0.211911	0.72123	1.2	10	0.89
0.04	0.0298044	0.224185	0.706011	1.2	12.5	
0.04	0.0327323	0.236385	0.690883	1.2	15	

[27].

Lewis number was defined as the ratio of the thermal diffusivity of a mixture to the mass diffusivity of a deficient gas component, that is, $Le = \alpha/D_{dif}$. For mixed fuel cases, the fuel Lewis number of a reactant was computed as a weighted average of the Lewis numbers of two fuels, given as follows [28-29]:

$$\mathrm{Le_F} = 1 + \frac{\mathrm{q_{C_2H_4}(Le_{C_2H_4} - 1) + q_{C_3H_8}(Le_{C_3H_8} - 1)}}{\mathrm{q}} \tag{4-1}$$

where $q_i = QY_{i,u}/cpT_u$ is the non-dimensional heat release rate associated with the consumption of species i, and $q = q_{C2H4}+q_{C3H8}$ is the total heat release. [28] Le_{C2H4}, Le_{C3H8} are the fuel Lewis numbers of each of the fuel gases.

The effective Lewis number was defined as the combination of the Lewis numbers of the fuel and the oxidizer [30], defined as follows:

$$\mathrm{Le}_{\mathrm{eff}} = 1 + \frac{(\mathrm{Le}_{\mathrm{E}} - 1) + (\mathrm{Le}_{\mathrm{D}} - 1)\mathrm{A}_1}{1 + \mathrm{A}_1} \tag{4-2}$$

where Le_E and Le_D are the Lewis numbers of the excessive and the deficient reactants, respectively. The parameter A_1 denotes mixture strength, and it is expressed as $A_1 = 1 + \beta(\Phi + 1)$, where Φ is the ratio of the mass of the excess to the deficient reactants in the mixture, and $\beta = Ea(T_{ad}-T_u)/R^0T^2_{ad}$ is the Zeldovich number, where T_{ad} is the adiabatic flame temperature, T_u the unburned gas temperature, $Ea = -2\,R^0[\partial\ln(\rho_u S^0_u)/\partial(1/T_{ad})]$ the activation energy, and R^0 the universal gas constant. As experimental parameters, we varied laminar burning velocity, input laser power, laser exposure time, and Lewis number. The range of input laser power was 2−18 W, and range of exposure time was 0.2−5 s.

4.1 Flame propagating behaviors with various laser irradiation condition in primary acoustic instability region

Figure 4.1 shows the typical downward flame propagation behavior under various laser exposure conditions in a tube. Once the flame was exposed to the external laser beam, the ethylene gas in the gas mixture absorbed laser energy, and subsequently, the preheated unburned mixture may have increased the local flame velocity. Then, the flame front structure deformed, as shown in Fig. 4.1 The convex curvature was generated immediately after laser exposure, and then, in a few cases, the concave structure of the flame front was formed (II). This concave structure was reported by K. Agular et al. in a previous study [24]. When the laser beam was irradiated onto the tube, the density discrepancy between the laser path and surrounding region was determined. In this scenario, buoyancy-induced flow can be generated. If the velocity of the buoyancy-induced flow is higher than the increment in burning velocity owing to laser beam absorption, the concave structure is generated, as shown in (II) of Fig. 4.1. However, in the short-term laser exposure cases, the concave structure was not developed because the density gradient was negligible, as shown in (IV) of Fig. 4.1

When the input laser power was sufficiently large, the transition to secondary acoustic instability occurred. In Fig. 4.1, the transition motions are classified into two types of behaviors. In one case, the flame transitioned from the concave structure into the corrugated structure with turbulent motion (Fig. 4.1. III), while in another case, the flame transitioned from the concave structure into the convex structure (Fig. 4.1 V). Now we consider the effect of *Le*. When *Le* is greater than unity, the concave flame tip is accelerated because the flame tip temperature

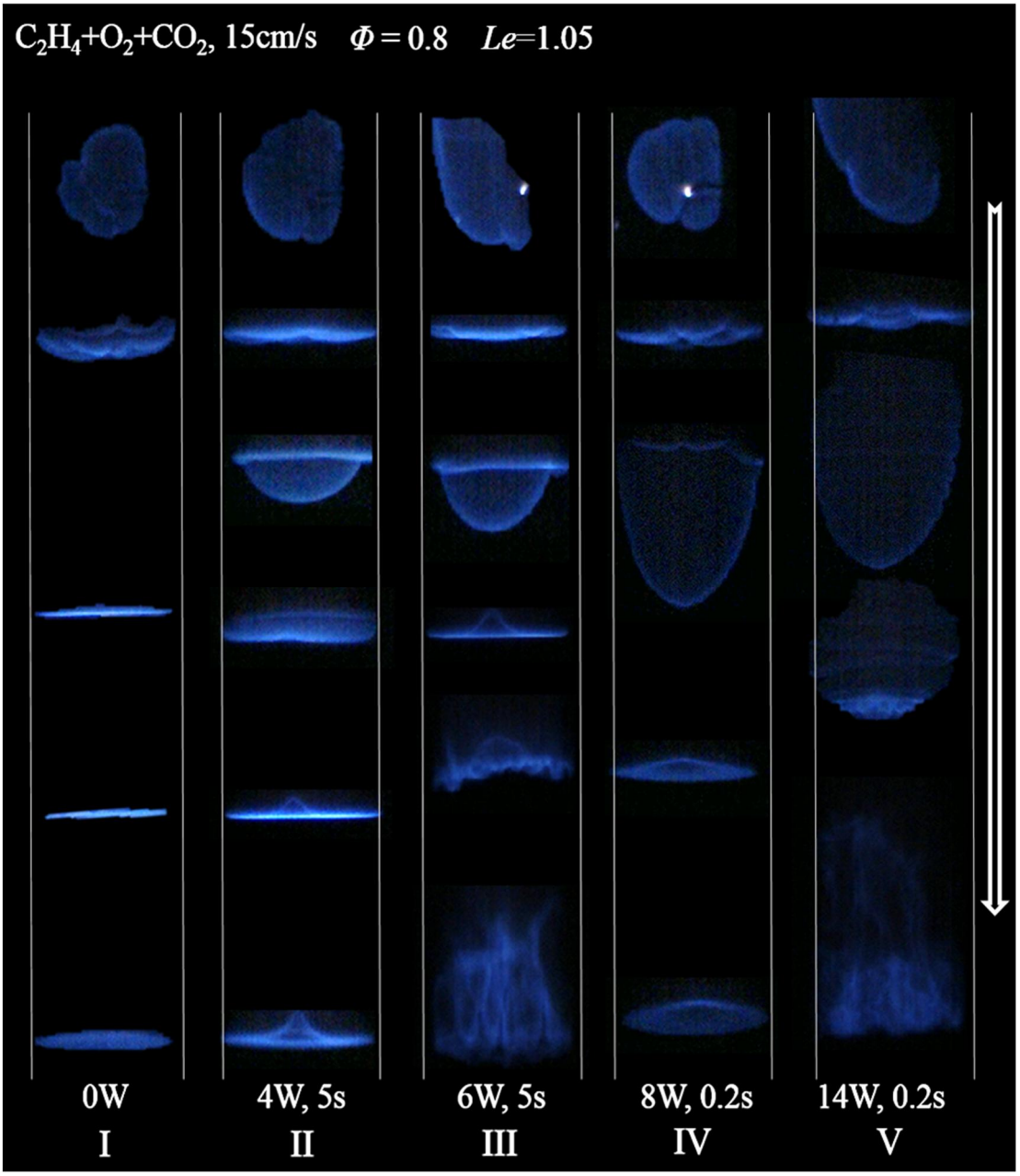

Figure 4.1. The flame propagation behavior in a tube with various laser exposure conditions

increases owing to enhanced heat conduction from surrounding burned gas, when *Le* is smaller than unity, the flame temperature decreases. Then, additional experiments were carried out under various *Le* conditions to clarify the effect of *Le* on the transition criteria in terms of laser power (vertical axis) and exposure time, and the resulting transition map was established, as shown in Chapter 4.2.

4.2 Variation of the transition criteria

4.2.1 Laser irradiation time effect

Figure 4.2 shows the critical input laser power for the flame structure transition as a function of the laser exposure time for both $Le < 1$ (a) and $Le > 1$ (b). The figure shows that the curve of $Le > 1$ contains two branches of critical input laser power, namely, the increasing branch and the decreasing branch with laser exposure time. That implies that different transition mechanisms exist as functions of laser exposure time. The transition behaviors of the increasing and decreasing branches are different, as shown in Figs. 4.1 (V) and 4.1 (III), respectively. Such distinct results could be explained by considering the flame front curvature and the thermal-diffusive effect as follows. In the short-term laser exposure cases, the flame front had a convex curvature because the time scale was too short to generate the concave structure (explanation is given below). Therefore, the flame experienced a stronger positive curvature with increasing exposure time; then, the local flame propagation velocity was accelerated for $Le < 1$ or decelerated for $Le > 1$. Consequently, when $Le > 1$, higher laser power is required for enabling the transition to overcome the negative effect of Le in case of the convex curvature. However, if sufficient exposure time is given to the mixture, the concave structure is developed because the premixed gas along the centerline is preheated and the upward buoyancy-induced flow starts to impart a concave structure to the flame front. Because the time scale of the buoyancy-induced flow generation is longer than the convex structure generation process, such concave structures are formed only after long laser exposure times. Under $Le > 1$, such generation of the concave structure makes the flame front more unstable, and lower laser power is required for the transition with increasing laser exposure time. In the case of $Le < 1$, the flame temperature increase owing to the convex curvature, and the transition appears at the very

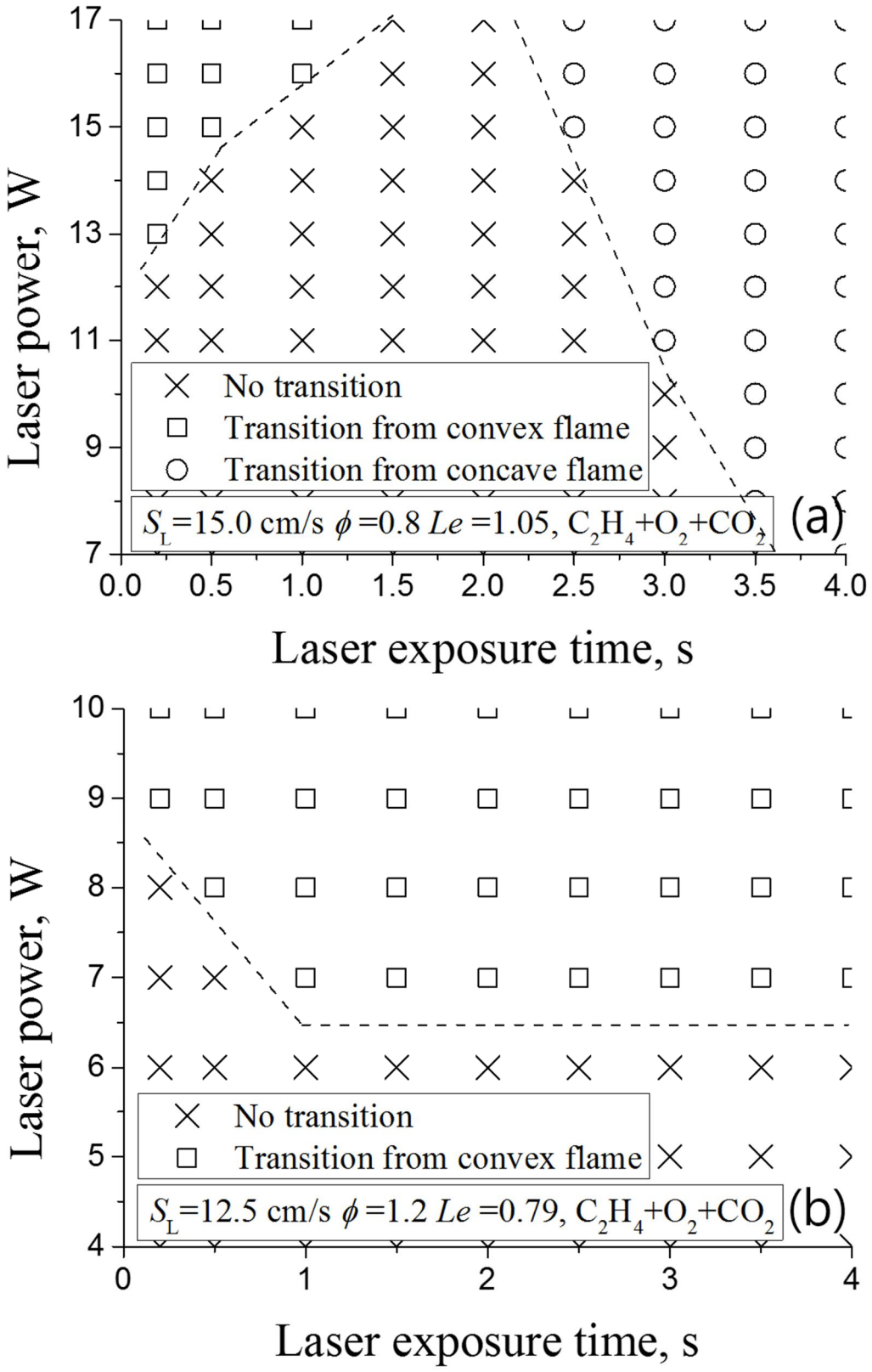

Fig. 4.2 The criteria of the transition to the secondary instability as a function of laser exposure time. (a) Le=1.05, (b) Le=0.79

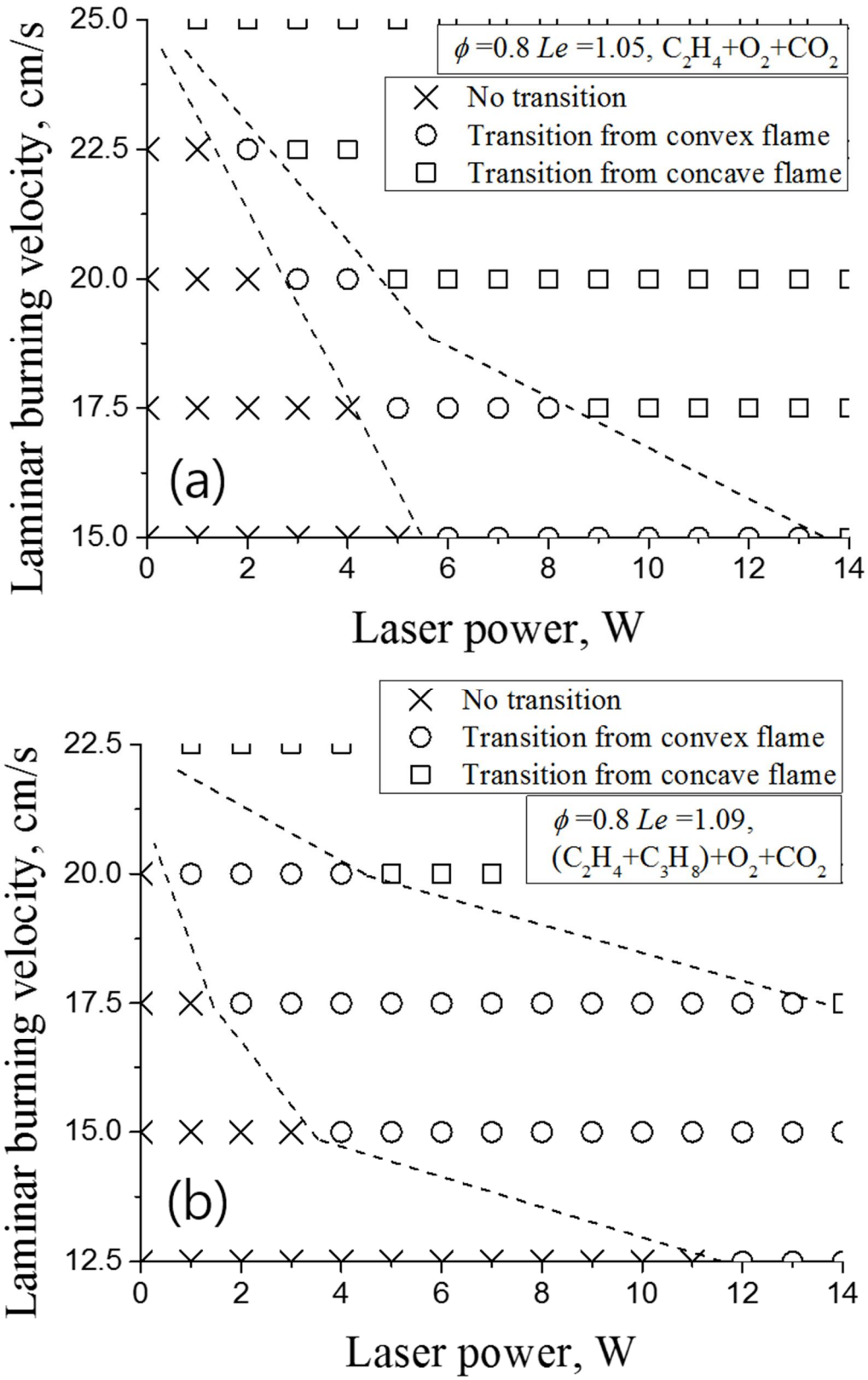

Fig. 4.3 The criteria of the transition to the secondary instability as a function of input laser power for Le>1. (a) single fuel (ethylene), (b) binary fuel (ethylene + propane).

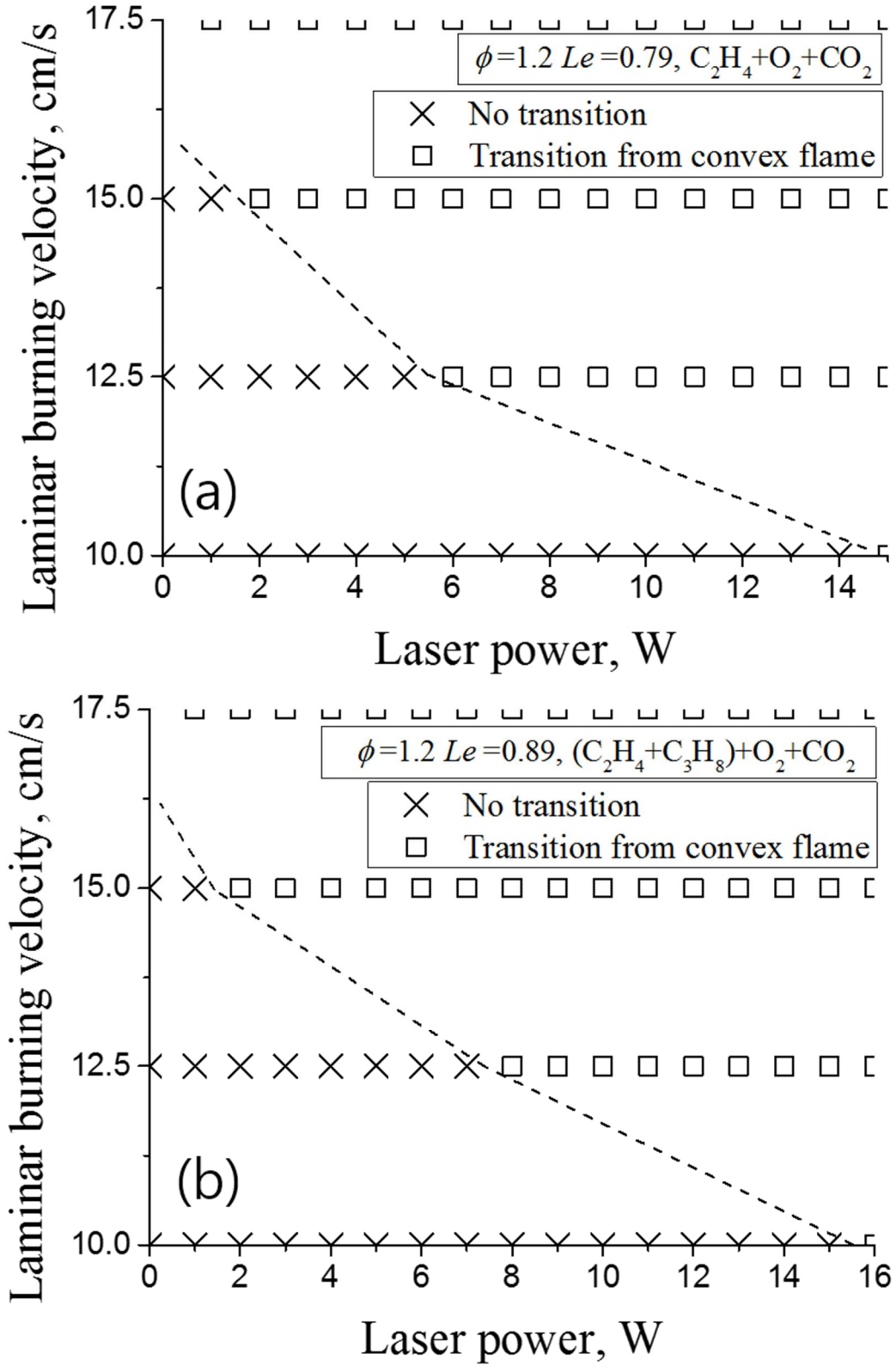

Fig. 4.4 The criteria of the transition to the secondary instability as a function of input laser power for Le<1. (a) single fuel (ethylene), (b) binary fuel (ethylene + propane).

initial moment after the start of laser exposure. In this scenario, the transition limit in terms of laser power does not change with the exposure time.

4.2.2 Input laser power effect

Figure 4.3 and 4.4 show the critical laminar burning velocity in case of the transition to the secondary acoustic instability for a given input laser power, laser exposure time (5 s), and various values of *Le*. The Fig. 4.3 (a) and 4.4 (a) are the result of the pure ethylene fuel case, and the Fig. 4.3 (b) and 4.4 (b) correspond to the binary fuel case (ethylene and propane). The closed plots denote the transition from the concave structure (Fig. 4.1 III), and the transition shown by the open plots are identical to that in Fig. 4.1 V. The transition behavior in the cases of $Le < 1$ (Fig. 4.4) were always the same as that in Fig. 4.1 (V) for both the binary and the single fuel cases. The mass diffusion of deficient reactant is more dominant in the condition of $Le < 1$. In this situation, once the convex curvature is formed, the flame tip temperature is raised by the focusing effect on the concentration of the deficient reactant approaching the flame.

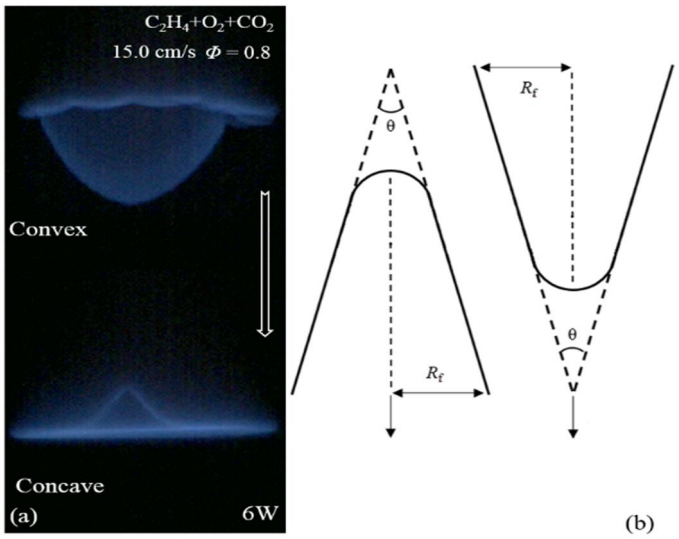

Fig. 4.5 (a) Direict image of flame front curvature with laser irradiation, (b) schematic drawing of flame front structure.

Thus, the transition occurs from the convex curvature flame or can be happen with concave structure which appears subsequent to the convex curvature.

However, when *Le* is larger than unity, the case of Fig. 4.1 (III) always appeared first as shown in Fig. 4.3, and then, if very high laser power was supplied, the transition behavior changed to the case shown in Fig. 4.1 (V). This result also could be understood as the thermal-diffusive instability effect in accordance with the discrepancy in flame front curvature with changing values of *Le*. For large Lewis number case (Fig. 4.3), the flame temperature rises with presence of concave curvature owing to the diffusively convergence of heat flux contrary to the convex structure. Thus, the transition can be taken place when the flame has the concave curvature only.

The concave transition region in the binary fuel cases is wider than the single fuel cases in Fig. 4.3. It is also explained by thermal diffusion process rather than the effect of preferential diffusion of two different fuels. Because if the larger diffusivity of ethylene had positive effect on the transition, the pure ethylene case should give earlier transition. Also, if the preferential diffusion had important effect, single and binary fuel cases should show clear difference even at Le<1, while the difference is very small as seen in Fig. 4.4. This fact implies that the ratio of thermal diffusivity to the diffusivity of deficient composition, O2 in this case, is the dominant factor rather than the mass diffusivity difference of individual fuels. The Lewis number for a fuel lean condition in this paper is larger for the binary fuel case than that of the pure ethylene case (1.09>1.05).

The transition criteria have very different sensitivity to the input laser power in terms of the transition modes as show in Fig. 4.3 and 4.4. Moreover, even with same input laser power, the amplitude of flame front curvature is quite different between the convex and concave flames,

as shown in Fig. 4.5 (a). To clarify more the effect of Lewis number on acoustic instability, the quantitative evaluation about effect of flame front curvature was conducted in the Section 4.3.

4.3 Quantitative evaluation of effect of flame curvature

Flame curvature significantly influences the structure and propagation of the premixed flame by way of its influence on flame stretch. Fig. 4.5 (b) shows a schematic drawing of the flame configurations for the concave and convex curvatures. If an axisymmetric cone-shaped flame structure is considered, the flame stretch rate attributed to the flame front curvature can be defined as follows [31]:

$$\kappa = \frac{u_0 \sin\theta}{2R_f} \tag{4-3}$$

where u_0 is the laminar burning velocity, θ the apex angle, and R_f the radius of a segment of the deformed flame. Note that the stretch rate is positive for a positive curvature toward the unburned mixture (convex), while $\kappa < 0$ for a negative flame front curvature (concave). The stretch rate was evaluated based on the above considerations, and the resulting values are listed in Table 2. The stretched flame propagation velocity (S_n) shares a linear relationship with the stretch rate according to the following equation:

$$S^1 - S_n = L_b\kappa \tag{4-4}$$

here, S^1 is the unstretched laminar burning velocity and L_b the Markstein length [32-35].

Table. 4.2 Flame stretch rate as a function of Eq. (4-3)

		15.0 cm/s			17.5 cm/s			20.0 cm/s
		2 W	4 W	6 W	2 W	4 W	6 W	2 W
Single fuel	Convex	2.469	2.770	3.640	2.611	3.035	3.270	2.691
	Concave	-9.455	-9.958	-13.306	-9.718	-11.110	-13.427	-6.648
Binary fuel	Convex	-	1.545	1.735	1.745	2.319	2.562	1.994
	Concave	-	-6.774	-8.820	-5.759	-6.967	-9.667	-5.880

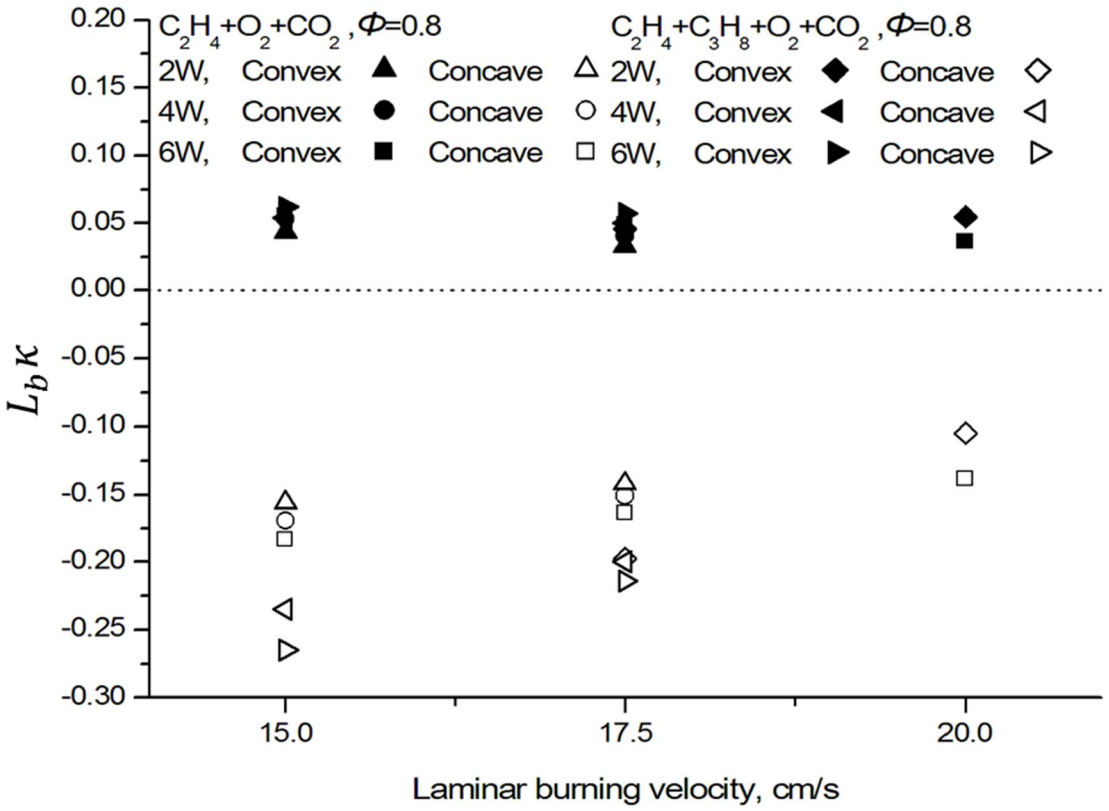

Fig. 4.6 Change in burning velocity cause by the presence of curvature as a function of S^l.

The Markstein number characterizes the effect of local heat release of a propagating flame on flame surface variation along the flame and the associated local flame front curvature. Clavin and Williams derived an expression for the value of the Markstein number considering high activation energy, small strain, and a one-step reaction [36]. Clavin and Garcia extended the aforementioned calculation to include the temperature dependence of diffusivities and suggested the following expression [37]:

$$Ma=\frac{1}{\gamma}J+\frac{\beta(Le-1)}{2}\left(\frac{1-\gamma}{\gamma}\right)D \tag{4-5}$$

$$J=\int_1^{\theta_b}\frac{h(\theta)}{\theta}d\theta$$

and

$$D = \int_1^{\theta_b} \ln\left(\frac{(\theta_b - 1)}{(\theta - 1)}\right) \frac{h(\theta)}{\theta} d\theta \quad (4\text{-}6)$$

where γ is the reduced gas expansion factor $(T_b\text{-}T_0)/T_b$, θ is the reduced temperature, $(T\text{-}T_0)/T_b$, $h(\theta)$ is the ratio of the thermal diffusivity at temperature θ to its value in the unburned gas, and β is the reduced activation energy of the reaction [38]. The Markstein number can be altered to the Markstein length in accordance with $Ma = L_b/l_f$. The flame stretch effect considering the Markstein length was evaluated based on the above consideration.

Fig. 4.6 shows the effect flame curvature on the change in laminar burning velocity. In the case of $Le > 1$, the effect of flame curvature was positive for the convex curvature and negative for the concave curvature. This implies that the flame velocity decreased in case of the convex structure and increased in case of the concave structure. Moreover, the result in case of the concave curvature was much higher than the that in case of the convex curvature, and it decreased significantly with the laminar burning velocity in case of the concave curvature but did not show any significant change in the convex curvature case. It implies that the effect of concave curvature is stronger than the convex curvature even under same input laser power and such relatively stronger curvature effect can cause more sensitive response of the transition criteria variation to input laser power. These results are well described by the effect of Lewis number on the transition criteria owing to the contribution of the flame curvature to the flame stretch rate.

4.4 Concluding remarks

In this chapter, we investigated the effect of Lewis number on the transition of a downward-propagating premixed flame in a tube from primary acoustic instability to secondary acoustic instability by controlling the flame front curvature. The flame front structure was changed from flat to curved by using the CO2 laser irradiation method. While the flame was propagated with laser exposure, both flame front curvatures (concave, convex) could be obtained.

Two types of transition behavior were observed: (1) transition from the concave flame front curvature and (2) transition from the convex structure immediately after laser irradiation. When the Lewis number was less than unity, only transition (2) occurred, but both transition modes were observed for $Le > 1$ with increasing laser exposure time. This result could be explained by the effect of thermal-diffusive instability depending on *Le*.

When *Le* was larger than unity, transition (1) always occurred first, then, the transition mode changed to transition (2) with adequate input laser power. Moreover, the transition in the binary fuel cases occurred at a lower input laser power condition than that in the single fuel cases. It was also confirmed that the effect of *Le* attributed to the flame curvature well underpinned the above result by evaluating the stretch effect ($L_b K$), and it was also confirmed that the effect of Lewis number due to the flame front curvature influenced the transition from primary acoustic instability to secondary acoustic instability.

Chapter 5 Summary

The experimental research of downward-propagating flame in a combustion tube is conducted. The main focus is to clarify the Lewis number effect on the acoustic instability and the transition criteria from primary acoustic instability to secondary acoustic instability. The flammable gas mixture was ignited at the top, open end of the tube, and a flame front propagated toward the closed end of tube. The flame behavior and acoustic pressure are measured.

The Chapter 3 deal with the effect of the Lewis number on acoustic instability of downward-propagating flame in a combustion tube through controlling flame front structure by CO_2 laser irradiation method. The investigation was conducted under two different Lewis number condition (1.05 and 0.79). The generation of larger convex curvature by laser irradiation can facilitate the rise of growth rate of acoustic pressure for Le<1, and the growth of acoustic pressure is suppressed accompanied with the convex structure for Le>1. The mechanism of diffusive thermal instability well describes the acoustic amplitude change in terms of flame front shapes. The thermal diffusion process is more dominant for Le>1 and hence the defocusing effect of heat flux is relatively stronger than the convergence effect of concentration of the deficient reactant. Therefore, the convex curvature for Le>1 brings about the suppression of growth of acoustic pressure. On the other hand, the concave curvature can be obtained by buoyancy induced flow subsequent to the generation of convex curvature with laser irradiation. Then, the heat flux converges from a large segment of reaction sheet upon diffusion zone. Thus, the flame temperature tends to be raised. The enhanced heat release from flame can amplify the acoustic wave and the transition from hydrodynamic instability region to primary acoustic instability region can be observed. For Le<1, the flame surface area

increased as the laser power rises and beginning of laser irradiation is earlier. The coupling constant, βM, is proportional to not only the growth rate of primary acoustic instability but the normalized flame surface area. Based on experimental results of $Le<1$, the normalized flame area was derived and linear relationship was obtained with the growth rate of acoustic pressure. In case of $Le>1$, the convex flame area increase did not cause the primary acoustic instability and the acoustic pressure amplification. However, the generation of concave flame induced the initiation of primary acoustic instability and its growth rate is proportional to the concave flame area. It clearly shows the *Le* effect on the acoustic instability.

In Chapter 4, we investigated the effect of Lewis number on the transition from primary acoustic instability to secondary acoustic instability by controlling the flame front curvature. The flame front structure was changed from flat to curved by using the CO2 laser irradiation method and both concave and convex curvature can be obtained.

Sufficient laser power is given, the transition occurs from primary acoustic instability to secondary acoustic instability and two types of transition behavior were observed: (1) transition from the concave flame front curvature and (2) transition from the convex structure immediately after laser irradiation. When the Lewis number was less than unity, the transition from convex structure can be observed only, however both transition modes were exist for $Le > 1$ with increasing laser exposure time.

For Le>1 transition (1) always occurred first, then, the transition mode was changed to transition (2) with adequate input laser power. The transition in the binary fuel cases occurred at a lower input laser power condition than that in the single fuel cases. It was confirmed that the effect of *Le* attributed to the flame curvature well underpinned the above result by evaluating the stretch effect ($L_b\kappa$), and it was also confirmed that the effect of Lewis number

due to the flame front curvature influenced the transition from primary acoustic instability to secondary acoustic instability.

References

[1] S. H. Chung, C. K. Law, Combust. Flame 55 (1984) 123-125.

[2] A. Levy, Proc. Roy. Soc. A283 (1965) 134.

[3] G. Darrieus, Unpublished work presented at La Technique Moderne, and at Le Congrés de Mécanique Appliqueée (1945).

[4] L. Landau, Acta Phys.-Chim. URSS 19 (1944) 77-85.

[5] J. Jarosinski, B. Veyssiere, Combustion phenomena, CRC Press, New York, 2009.

[6] G. Searby, Proc. Int. Conf. Combust. Detonation, Zel'dovich Memorial II (2004).

[7] J. Rayleigh, Nature. 18 (1878) 319.

[8] R.A. Dunlap. Resonance of flames in a parallel-walled combustion chamber. Technical Report Project MX833, Report UMM-43, Aeronautical Research Center. University of Michigan, 1950.

[9] A. van Harten, A.K. Kapila, and B. J. Matkowsky. Acoustic coupling of flames. SIAM Journal on Applied Mathematics, 44(5):982–995, 1984. doi: 10.1137/0144069. URL http:// link.aip.org/link/?SMM/44/982/1.

[10] P. Clavin, P. Pelcé, and L. He. One-dimensional vibratory instability of planar flames propagating in tubes. Journal of Fluid Mechanics, 216:299–322, 1990.

[11] A.C. McIntosh. Pressure disturbances of different length scales interacting with conventional flames. Combustion Science and Technology, 75:287–309, 1991.

[12] A.C. McIntosh. The linearised response of the mass burning rate of a premixed flame to rapid pressure changes. Combustion Science and Technology, 91:329–346, 1993.G. I. Sivashinsky, Rev. Fluid. Mech. 15 (1983) 179-199.

[13] A.C. McIntosh. The linearised response of the mass burning rate of a premixed flame to rapid pressure changes. Combustion Science and Technology, 91:329–346, 1993.H. Pearlman, P. Ronney, Physics of Fluids 6 (12) 4009-4018.

[14] A.A. Putnam and R.D. Williams. Organ pipe oscillations in a flame filled tube. Proceedings of the Combustion Institute, 4:556–575, 1952.

[15] G.H. Markstein. Flames as amplifiers of fluid mechanical disturbances. In Proceeding of the sixth National congress for Applied Mechanics, Cambridge, MA, pp. 11–33, 1970.

[16] G. Searby and D. Rochwerger. A parametric acoustic instability in premixed flames. Journal of Fluid Mechanics, 231:529–543, 1991.

[17] P. Pelcé and D. Rochwerger. Vibratory instability of cellular flames propagating in tubes. Journal of Fluid Mechanics, 239:293–307, 1992.

[18] G. Searby, Combust. Sci. and Tech. 81 (1992) 221-231.

[19] W. E. Kaskan, Proc. Combust. Inst. 4 (1953) 575-591.

[20] D. Bradley, Internal Combustion Engineering: Science and Technology (J Wearing, Ed.), Elsevier Applied Science, London (1990) 287-331.

[21] M. Tsuchimoto, O. Fujita, T. Honko, Y. Nakamura, H. Ito, Proc. Combust. Inst. 32 (2009) 1003-1009.

[22] J. S. Park, O. Fujita, Y. Nakamura, H. Ito, Proc. Combust. Inst. 33 (2014) 1105-1112.

[23] Y. Taniyama, O. Fujita, Combust. Flame 161 (6) (2014) 1558-1565.

[24] K. Aguilar, Y. Taniyama, H. Ito, O. Fujita, Combust. Sci. Technol. 186 (10-11) (2014) 1434-1446.

[25] The national institute of standards and technology (NIST), available at <hittp://webbook.nist.gov/chemistry/>.

[26] R. J. Kee, R. M. Rupley, et al., CHEMKIN PRO, Reaction Design, Inc., San Diego, CA, 2009.

[27] A. K. Dubey, Y. Koyama, N. Hashimoto, O. Fujita, Proc. Combust Inst. in press, https://doi.org/10.1016/j.proci.2018.06.155

[28] C. K. Law, G. Jomaas, J. K. Bechtold, Proc. Combust. Inst. 30 (2005) 159-167

[29] C. Tang, Z. Huang, J. Wang, J. Zheng, Int. J Hydrogen Energy 34 (5) (2009) 2483-2487.

[30] R. Addabbo, J. K. Bechtold, M. Matalon, Proc. Combust. Inst. 29 (2002) 1527-1535.

[31] C. K. Law, Proc. Combust. Inst. 22 (1988) 1381-1402.

[32] N. Peters, F. A. Williams, Combust. Flame 68 (1987) 185-207.

[33] P. Clavin, Prog Energy Combust. Sci. 11 (1985) 1-59.

[34] D. Bradley, P. H. Gaskell, X. J. Gu, Combust. Flame 104 (1-2) (1996) 176-198.

[35] D. Bradley, R. A. Hicks, M. Lawes, C. G. W. Sheppard, R. Woolley, Combust. Flame 115 (1-2) (1998) 126-144.

[36] P. Clavin, F. A. Williams, J. Fluid Mech. 116 (1982) 251-282.

[37] P. Clavin, P. Garcia, J. Méc. Théor. Appl. 2 (1983) 245-263.

[38] G. Searby, J. Quinard, Combust. Flame 82 (1990) 298-311.

Achievements

Journal publications:

1. **Y. H. Chung**, O. Fujita, N. Hashimoto, "Effect of Le on criteria of transition to secondary acoustic instability of downward-propagating flame in a tube with controlled curvature induced by external laser", ***Proceedings of the Combustion Institute***, in press, https://doi.org/10.1016/j.proci.2018.06.159

Conference publications:

1. **Y. H. Chung**, N. Hashimoto, O. Fujita, "Transition to secondary acoustic instability induced by external laser irradiation in a tube", ***55th Symposium (Japanese) on Combustion***, Toyama, Japan, (2017. 11, Oral presentation).
2. **Y. H. Chung**, N. Hashimoto, O. Fujita, "Effect of Le on criteria of transition to secondary acoustic instability of downward-propagating flame in a tube with controlled curvature induced by external laser", ***37th International Symposium on Combustion***, Dublin, Ireland, (2018. 8, Oral presentation).
3. **Y. H. Chung**, N. Hashimoto, O. Fujita, "Le effect on primary acoustic instability of downward propagating flame in a tube with external laser irradiation method", ***56th Symposium (Japanese) on Combustion***, Osaka, Japan, (2018. 11, Oral presentation, To be presented).